REFERENCE COPY

UNCLASSIFIED

NATIONAL AERONAUTICS AND SPACE ADMINISTRATION

Space Programs Summary 37-43, Vol. II

LAB-D00524

The Planetary–Interplanetary Program

For the Period November 1 to December 31, 1966

(Title Unclassified)

Classification Changed to UNCLASSIFIED
Authority NASA-Langley
By authority of signed by W. E. Hanson
Date
By

Copy No. 430

JET PROPULSION LABORATORY
JET PROPULSION LABORATORY LIBRARY
CALIFORNIA INSTITUTE OF TECHNOLOGY
PASADENA, CALIFORNIA
APR 7 1967
CALIFORNIA INSTITUTE OF TECHNOLOGY

January 31, 1967

UNCLASSIFIED

155481

UNCLASSIFIED

SPACE PROGRAMS SUMMARY 37-43, VOL. II

Copyright © 1967
Jet Propulsion Laboratory
California Institute of Technology

Prepared Under Contract No. NAS 7-100
National Aeronautics and Space Administration

This document contains information affecting the national defense of the United States, within the meaning of the Espionage Laws, Title 18, U.S.C., Sections 793 and 794, the transmission or revelation of which in any manner to an unauthorized person is prohibited by law.

GROUP 4 Downgraded at 3 year intervals; declassified after 12 years.

CONFIDENTIAL
UNCLASSIFIED

UNCLASSIFIED

Preface

The Space Programs Summary is a six-volume bimonthly publication designed to report on JPL space exploration programs and related supporting research and advanced development projects. The titles of all volumes of the Space Programs Summary are:

Vol. I. *The Lunar Program* (Confidential)
Vol. II. *The Planetary–Interplanetary Program* (Confidential)
Vol. III. *The Deep Space Network* (Unclassified)
Vol. IV. *Supporting Research and Advanced Development* (Unclassified)
Vol. V. *Supporting Research and Advanced Development* (Confidential)
Vol. VI. *Space Exploration Programs and Space Sciences* (Unclassified)

The Space Programs Summary, Vol. VI, consists of an unclassified digest of appropriate material from Vols. I, II, and III; an original presentation of the JPL quality assurance and reliability efforts, and the environmental- and dynamic-testing facility-development activities; and a reprint of the space science instrumentation studies of Vols. I and II.

Approved by:

W. H. Pickering, *Director*
Jet Propulsion Laboratory

UNCLASSIFIED

UNCLASSIFIED
CONFIDENTIAL

Contents

I. *Mariner IV* Project 1
A. Introduction 1

II. *Mariner* Venus 67 Project 2
A. Introduction 2
B. Project Engineering 3
C. Systems 4
D. Engineering Mechanics 5
E. Guidance and Control 9
References 21

III. *Mariner* Mars 1969 Project 22
A. Introduction 22
B. Project Engineering 23
C. Systems 23
D. Guidance and Control 34
Reference 34

IV. *Voyager* Project 35
A. Introduction 35
B. Guidance and Control 36

V. Future Projects 42
A. Introduction 42
B. A Comet Mission 42

UNCLASSIFIED
CONFIDENTIAL

UNCLASSIFIED
CONFIDENTIAL

I. *Mariner IV* Project

A. Introduction

The *Mariner IV* Project is under the administrative cognizance of the *Mariner* 1967 Project Office, which also directs the *Mariner* Venus 67 Project and the residual activity of the *Mariner* Mars 1964 Project. Residual activity of the *Mariner* Mars 1964 Project consists primarily of continuing analysis of tracking data, publication of results by the principal investigators, and preparation of final reports. However, periodic detection, recording, and commanding activities involving the *Mariner IV* spacecraft have been assigned to the Deep Space Network (DSN). Elements of the experimental facilities at Goldstone Station (DSS 13 and 14) have been used to successfully communicate with the spacecraft. The DSN results will be published periodically in Vol. III of future Space Programs Summaries. *Mariner* Venus 67 Project activities are reported in the following Section II.

The objectives, authorized in December 1965, simultaneously with those for the Venus flight, have been established as:

The primary objective of the Mariner IV Project is to obtain scientific information on the interplanetary environment in a region of space further from the Sun than the orbit of Earth during a period of increasing solar activity in 1967, using the Mariner IV spacecraft still operating in orbit around the Sun.

The secondary objectives are to obtain additional engineering knowledge about the consequences of extended exposure of spacecraft equipment in the interplanetary space environment and to acquire experience in the operation of a planetary spacecraft after a prolonged lifetime in deep space.

During this reporting period, the Mars Station R&D facility (DSS 14) acquired telemetry data (totaling 16 hr) from *Mariner IV* on December 2, 15, and 21. A carrier level of −168.5 dbm was observed December 21. An equipment failure in the special data-handling provision was corrected and typical processing activities were resumed.

CONFIDENTIAL
UNCLASSIFIED

UNCLASSIFIED

II. *Mariner* Venus 67 Project

A. Introduction

The *Mariner* Venus 67 Project is under the administrative cognizance of the *Mariner* 1967 Project Office, which is also responsible for the *Mariner* Mars 1964 Project and the *Mariner IV* Project (see Section I).

1. *Mariner* Venus 67 Project

The major task of the *Mariner* 1967 Project is the Venus flyby mission, named the *Mariner* Venus 67 Project. The following mission objectives have been established:

> *The primary objective of the Mariner Venus 67 Project is to conduct a flyby mission to Venus in 1967 in order to obtain scientific information which will complement and extend the results obtained by Mariner II relevant to determining the origin and nature of Venus and its environment.*
>
> *Secondary objectives are to acquire engineering experience in converting and operating a spacecraft designed for flight to Mars into one flown to Venus, and to obtain information on the interplanetary environment during a period of increasing solar activity.*

With the authorizing of this project late in December of 1965, and the launch opportunity occurring in June 1967, the period available to the *Mariner* Venus 67 Project for planning, design, test, and other flight preparation is 18 mo. Because of this minimum length of time, application, to the fullest extent possible, must be made of techniques developed from the experience of prior missions, and existing hardware must be utilized.

The single flight spacecraft, designated M67-2, is currently being prepared by converting the spare spacecraft (MC-4) that was built for the *Mariner* Mars 1964 Project.[1] An *Atlas-Agena D* launch vehicle will inject the spacecraft into a 120-day transit trajectory. The launch readiness date has been set at June 10, 1967, with a 14-day launch period starting June 12. Ranging provisions have been authorized for this mission which will offer the possibility of considerably enhancing the celestial mechanics experiment. At encounter, an unusually sharp perturbation will occur.

[1]Portions of the proof test model (PTM) spacecraft and spares from the MM64 Project are also being prepared as a flight-support spacecraft (M67-1); there will be no PTM as such. The flight-support spacecraft will serve the double function of pseudo-PTM and backup spacecraft for qualifying spare subsystems.

UNCLASSIFIED

UNCLASSIFIED

Seven scientific experiments have been approved for the *Mariner* Venus 67 mission:

Experiment	*Principal investigator*
S-band radio occultation	Arvydas J. Kliore, Jet Propulsion Laboratory
Ultraviolet photometer	Charles A. Barth, University of Colorado
Dual-frequency radio propagation	Von R. Eshleman, Stanford University
Helium magnetometer	Edward J. Smith, Jet Propulsion Laboratory
Solar plasma	Herbert S. Bridge, Massachusetts Institute of Technology
Trapped radiation	James A. Van Allen, State University of Iowa
Celestial mechanics	John D. Anderson, Jet Propulsion Laboratory

The first experiment requires the use of only the RF transmission subsystem on the spacecraft, and the last one utilizes only the tracking doppler data received from the RF carrier. Of the remaining five experiments, four are to be accomplished with the existing instrumentation, with only minor modifications. Only the dual-frequency radio propagation experiment of Stanford University requires the incorporation of a new scientific instrument into the payload.

Other changes to the basic spacecraft design are necessitated by the fact that the spacecraft will travel toward, rather than away from, the Sun and also because conversions must be made to accommodate revised encounter sequencing and science payload. In particular, modifications are needed in the following areas:

(1) Scientific data automation system

(2) Antenna pattern and orientation

(3) Thermal control

(4) Solar panel configuration

(5) Planetary sensors

During the November–December reporting period, delivery of all flight-quality hardware (telecommunications and science) for the M67-1 spacecraft was successfully accomplished. It is anticipated that delivery of all subsystems for the M67-2 spacecraft will be completed in late January. Assembly and check out of the M67-2 spacecraft will proceed generally along original plans with late subsystems being integrated as they become available.

Radio-frequency interference problems associated with the spacecraft system dual-frequency receiver have been corrected through various design changes. While it is felt that these changes have solved the problem, final verification can not be made until measurements on the *Mariner* Venus 67 spacecraft have been obtained.

Effectiveness of a retro maneuver and increased injection error due to the Sun in the field of view of the horizon sensors necessitated a restudy of these areas. The results of the study show that the 3-σ maneuver (with one sensor off) will be increased by 6 m/sec and bias will be on the order of 10 to 12 m/sec on each day of the launch window.

The shroud and adapter match-mate tests (using *Agena* interface test hardware) have been satisfactorily completed.

B. Project Engineering

1. Atlas/Agena Performance Predictions

During the fourth quarter of 1966 the tag values of the specific impulse for the *Mariner* Venus 67 launch vehicle have been decreased for both the *Atlas* and the *Agena*. The reduction in predicted *Agena* engine performance arose from a statistical study of a large volume of telemetry and radar tracking data from past flights. The decrease in specific impulse amounted to 1.70 sec for the *Agena*. This is equivalent to 25 lb of allowable payload for the *Mariner* Venus 67 mission.

The *Atlas* MA-5 engine sets are tested by Rocketdyne and the measured specific impulse (tag values) are supplied to General Dynamics/Convair (GD/C). Recent engine sets have shown higher performance than previously. Yet when GD/C ran computer simulations based on preflight and postflight data for recent launches, the higher specific impulse values could not be substantiated in the mathematical model. The model for the engines alone contains 12 variables.

Because the higher specific impulse values were inconsistent with results of the simulation model, GD/C is reducing the Rocketdyne tag values by 1.24 sec. This is

UNCLASSIFIED

UNCLASSIFIED

equivalent to 12.4 lb of allowable payload for the *Mariner* Venus 67 mission.

C. Systems

1. Systems-Test-Complex Data System

In this reporting period the systems-test-complex data system (STCDS) began active support of spacecraft system testing by use of the telemetry data processing capability of the system. This includes processing and display on a line printer of the science data automation system (DAS) data outputs to the data encoder and to Tracks 1 and 2 of the spacecraft tape recorder.

Provision of the events/status signal data processing capability is presently behind schedule, and approximately 50% of the interfaces and the associated special processing programs were checked out at the end of this reporting period. This lag is caused by late definition of the operational support equipment (OSE)-to-STCDS interface circuitry, and unavailability of the spacecraft for purposes of STCDS interface testing and program checkout.

The current status of the data input subsystem (DIS), located on the system test complex, is shown in Fig. 1. The left-hand rack (Rack 1) will contain the low- and high-speed analog data input modules, which are now delivered and installed, but are not shown in this figure. The 12

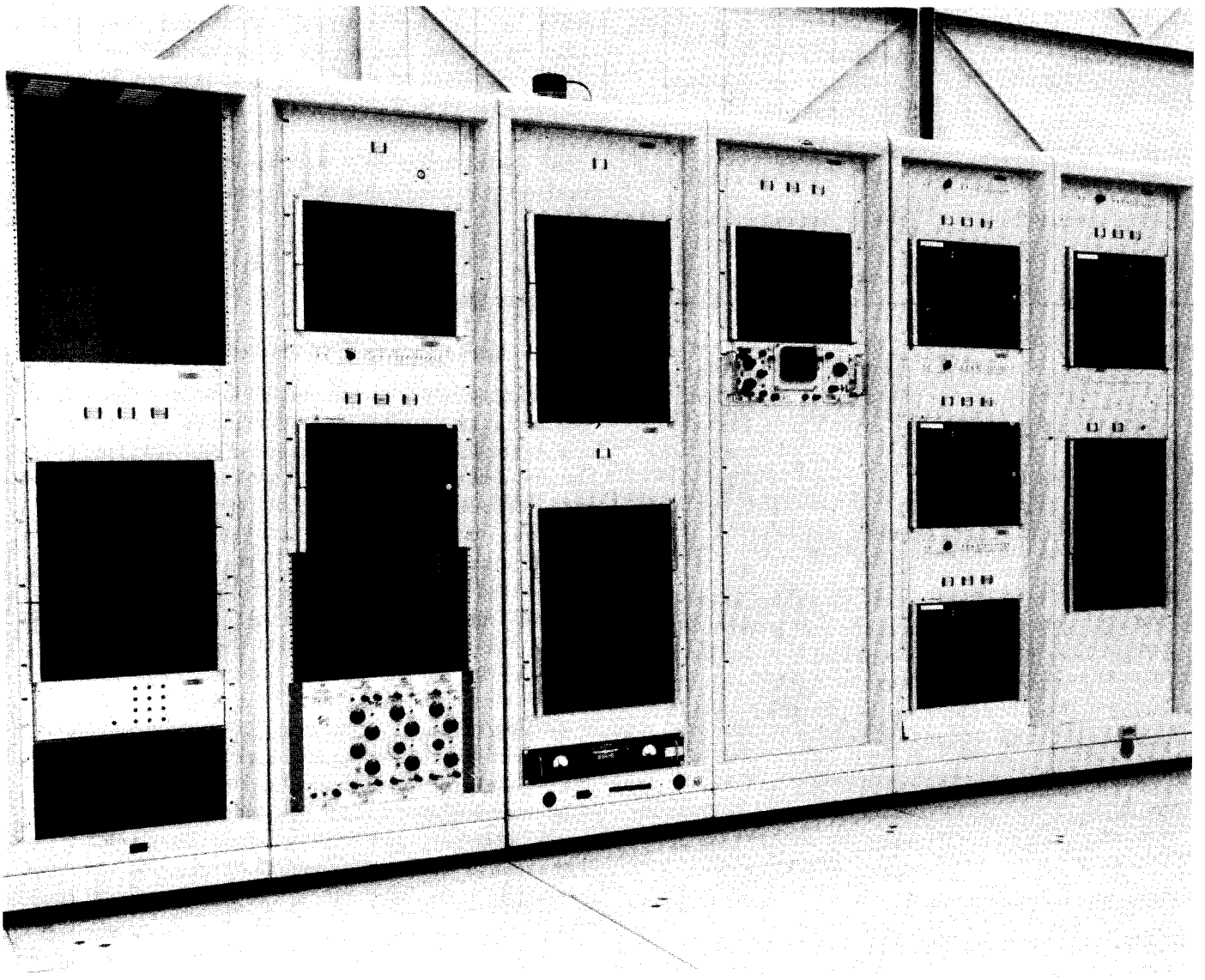

Fig. 1. Data input subsystem

UNCLASSIFIED CONFIDENTIAL

UNCLASSIFIED
CONFIDENTIAL

signal amplifiers for the analog modules are scheduled for delivery at the end of the reporting period. Rack 2 contains a diagnostic test module, which is a computer-controlled stimulus generator being developed for purposes of testing all other modules in the system, including the computer system input/output communication channels. A DAS data input module is located below the test module. Rack 3 contains two events/status data input modules and a power supply for interface circuitry. Rack 4 contains the counters module, a monitoring oscilloscope, and the junction box module, covered by a large panel,which terminates all of the OSE interface circuits. Rack 5 contains two additional DAS data input modules and a telemetry data input module. Rack 6, on the right, houses a telemetry input module and the DIS controller, which is the interface element between the CDC 3300 computer system and the DIS. The controller also contains the real-time clock buffer, which acquires STC time with 1-msec resolution for input to the computer. The telemetry data input and DAS data input modules are basically similar except for differences necessary to interface with data and sync lines of different level and format.

Several versions of the system test support program, each with somewhat increasing capability, were developed, tested, and used for processing spacecraft system test data. The capability for nonreal-time STCDS data processing is now available, which permits test data recorded on the STCDS log tape to be processed following a test. A real-time magnetic tape record called STET (system test experimenters tape), containing DAS and science telemetry outputs in a special format for science users, is now provided during all tests. An off-line program called XRPT (experimenters reformatting program for test data) is being developed for use on computer systems other than the CDC 3300 to allow extraction of data from the STET tape by experimenters or other users (refer to SPS 37-42, Vol.II p. 3).

D. Engineering Mechanics

1. Introduction

The last of the flight hardware for *Mariner* Venus 67 has been delivered to the Spacecraft Assembly Facility. A second structural vibration qualification test on the structural test model (STM) has been performed. This test supplemented the first test (SPS 37-41, Vol. II) conducted 4 mo earlier.

After the first STM test, the solar panel dampers, which hold the panels in the stowed position during boost, were found to have deteriorated. Gross leakage of the silicone oil from the dampers also occurred. The dampers, modified to correct these deficiencies, successfully requalified during the second series of STM vibration tests.

During boost, a deployable thermal sunshade is stowed within the *Agena* adapter. It is attached to each solar panel by lanyards which release the shade at panel deployment. A series of tests was conducted to determine the effects of a premature sunshade deployment while the spacecraft is still attached to the *Agena*. The results indicate that the spacecraft will successfully separate from the *Agena*, that the tumbling rates will be acceptable, and that the sunshade will not be affected detrimentally.

Additional tests were performed to test nominal sunshade deployment and to investigate deployment failure modes. These tests demonstrated adequate shade deployment mechanization.

During the temperature control model (TCM) tests in the space simulator, the readings from the two instruments used to measure the solar intensity differed by approximately 15%. To resolve this anomaly and to increase the assurance that the flight spacecraft will be tested at the correct solar intensity, a radiometer comparison test was conducted in the 10-ft Space Simulator. The results indicate that the cone radiometer, a device used during the TCM simulator test, gave readings that were substantially correct. It will be used to set the intensity levels for the flight spacecraft.

A thermal analysis has been performed to determine the worst-case thermal effect of the planet Venus at encounter on the *Mariner* Venus 67 spacecraft. The transient temperature rise of the solar panels and bus electronics will be less than 15°F and 5°F, respectively.

2. Structural Test Model Vibration Qualification Testing

The *Mariner* Venus structural test model has been subjected to a second composite vibration test, the purposes of which were: (1) to obtain supplemental dynamic response data required by recent design changes in the basic spacecraft structure; (2) to qualify structural hardware which was either not included in, or was modified since, the previous tests; and (3) to verify the complex wave vibration control equipment operational procedure to be used for the flight spacecraft vibration testing.

The modified STM successfully withstood the qualification dynamic loads defined in JPL Specification MVB-

UNCLASSIFIED
CONFIDENTIAL

50587-TST. Low frequency structural and complex wave qualification level excitations were introduced to the test structure along two lateral, and one axial, axes of the spacecraft. Analysis of reduced test data indicates no major changes in the dynamic response characteristics of the modified test structure. The STM underwent forced vibration excitation for a total of 60 min during the test period.

3. Solar Panel Boost Dampers

Boost dampers of the design reported in SPS 37-39, Vol. II, were fabricated and subjected to type-approval tests during the first series of STM vibration qualification tests. During the ultimate load level portion of the test series, the dampers "bottomed out" at end of travel at approximately 10 cps. Inspection of accelerometer data indicated that the impact energy was quite small and would not be detrimental to the hardware. In addition, because the required redesign would undoubtedly alter the damping properties at other frequencies, thus invalidating existing test data, it was concluded to accept this behavior.

Following the STM test series, a visual inspection of the dampers installed on the spacecraft indicated gross leakage of silicone oil from the damper assembly. The dampers were removed and bench-tested on a force-response machine to compare damping characteristics with data obtained prior to the STM environment. This test indicated an approximate 40% loss in damping. Examination of the disassembled dampers revealed extensive O-ring damage consisting of extrusion and tearing as the O-rings were forced out of their grooves. The obvious result of such damage would be the oil leakage and loss of damping properties observed.

As a consequence of these problems, the dampers were modified to eliminate O-ring wear and to improve their oil-sealing ability. The resultant configuration is depicted in Fig. 2. The first modification was the revision of piston/cylinder clearances and O-ring groove dimensions to a more conventional high-pressure seal design accommodating a standard size O-ring. In addition, the existing oil reservoir grooves were modified to allow a second in-series O-ring to be installed with a high-pressure backup ring. A new reservoir groove was then added to the center of the piston.

This new seal design successfully passed a series of extensive bench tests, the second series of STM/vibration tests, and an assembly level thermal vacuum/thermal

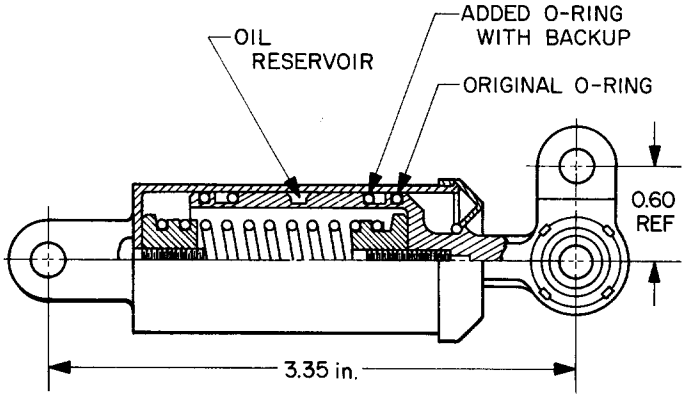

Fig. 2. Solar panel boost damper

shock test. The damper damping response did not appreciably deteriorate; no bottoming was observed during STM test; there was no detectable oil leakage.

4. Deployable Sun Shade Testing

All developmental and failure mode testing of the mechanical aspects of the deployable sunshade described in SPS 37-41, Vol. II, has been completed. A summary of the most recent tests and the results obtained follows.

a. Sun shade-Agena adapter interference tests

Preliminary test. A series of tests with the *Mariner* Venus 67 structural test model (STM) and an *Agena* adapter was performed. The purpose of these tests was to investigate the failure modes of a premature sunshade deployment prior to spacecraft separation from the *Agena* adapter and the effect on spacecraft separation. The spacecraft was hoisted from the adapter with the sunshade in various deployed conditions. Hoist loading was monitored with a load cell and recorded on an oscillograph.

A total of seven separations was performed. With the shade deployed in the adapter, severe shade hangup on the in-flight disconnect bracket was observed at separation (Fig. 3). Temporary snagging also occurred on the pyro arming switch (PAS) bracket and the push-off springs. Conservative analysis of the rather crude load cell data indicated that the spacecraft would separate from the *Agena* but that tip-off tumbling rates as high as 8 deg/sec might result from such hangups.

As a result of this test, protective shields on the in-flight disconnect and the PAS bracket were added to the adapter by Lockheed and a second pull test was scheduled.

UNCLASSIFIED
CONFIDENTIAL

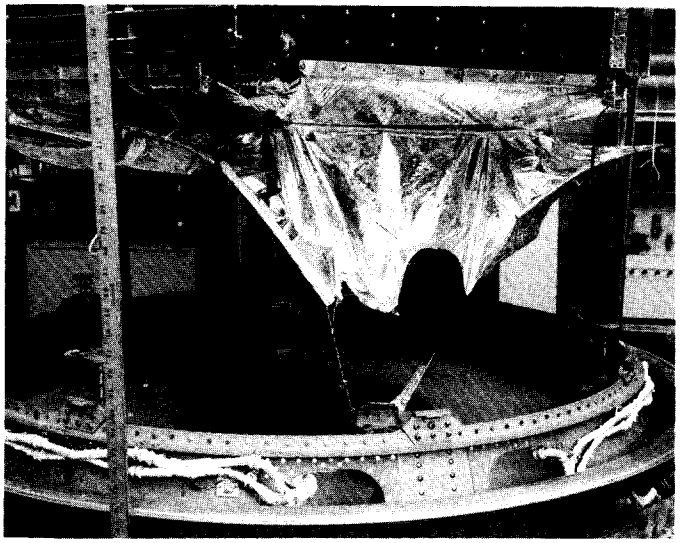

Fig. 3. Deployable Sun shade hangup

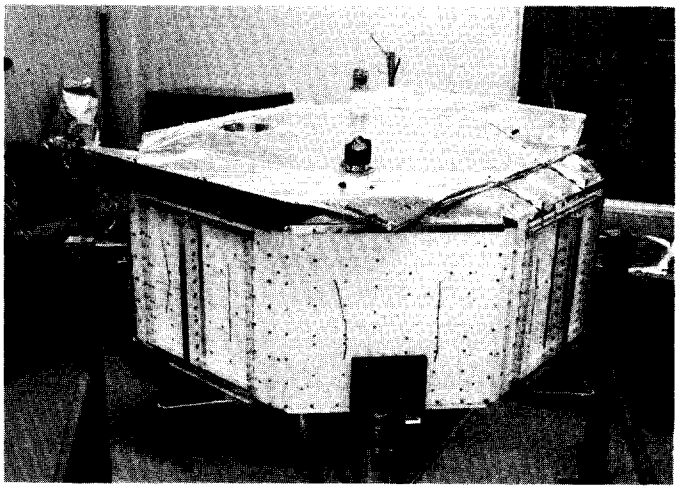

Fig. 4. Sun shade deployment test setup

Final test. The test setup and hardware used for the final test were essentially identical to those used for the first test, except that accelerometers were attached to the spacecraft to obtain tip-off rates. Also, the Lockheed-designed sunshade guides were affixed to the PAS and in-flight disconnect brackets.

A total of five separations was performed. With the shade prematurely deployed in the adapter, a slight hangup on one of the push-off springs occurred, bending one of the sunshade support tubes approximately 1 in. out of plane. Less severe temporary snagging was noted on the other three springs. If this were to happen in flight, the function of the sunshade and spacecraft would not be impaired. From the more accurate accelerometer data, the maximum tip-off rate due to the shade hangup was computed to be 2.1 deg/sec., an acceptably small effect.

b. Sun shade deployment test. A series of sunshade deployment tests was performed on a type-approval sunshade. The purpose was to test a nominal sunshade deployment and to investigate deployment failure modes. The spacecraft was mounted on a modified solar panel stand and could rotate 360 deg about a horizontal axis through Bays 4 and 8 (Fig. 4). The spacecraft was rotated in 90-deg intervals to four positions during the test to study gravity effects on the deployment mechanics. A simulated solar panel attach point was used to release the shade lanyard at the correct location and rate.

A total of 15 fully and partially deployed tests was performed. No anomalies occurred during standard deployment modes. During failure mode investigation it was established that the maximum force to release the Teflon "shirt tail" retainer ball should not exceed 150 g. The shirt tail is that part of the sunshade between the rigid support rods at the four corners of the stowed sunshade. The shirt tail is folded under and restrained by a lanyard and a ball which rests in a detent. The ball is pulled from the detent at shade deployment. It was also verified that when a single bay fails to deploy, the adjacent loose material (shirt tail) will be adequately restrained by the ball-detent. This retention is required to prevent sunlight reflections into Sun sensor cavities.

The test demonstrated adequate shade deployment mechanization. Shirt-tail retainer release force, a critical factor in assuring successful deployment, was established at 130 $\pm$10 g.

5. Space Simulator Radiometer Comparison Test

During the temperature control model (TCM) test in the 10-ft Space Simulator (SPS 37-41, Vol. II), the Eppley and absolute cavity (cone) radiometers used to monitor solar intensity differed by approximately 15% at Venus levels. Although the cone radiometer had been believed to be the more accurate instrument, it was observed that the ratio of the measured intensity to the lower thermal shield absolute temperature to the fourth power was not constant over the intensity range of the test. To resolve this anomaly and to increase the assurance that the flight spacecrafts would be tested at the correct solar intensities, a radiometer comparison test was conducted in the 10-ft Space Simulator.

UNCLASSIFIED
CONFIDENTIAL

UNCLASSIFIED
CONFIDENTIAL

The comparison test included the following items:

Item	Description
1	Eppley radiometer with 7-deg view limiter
2–7	Hycal radiometers
8–9	Cone radiometers
10	TCM lower thermal shield
11–12	Relative intensity monitors (RIM)
13–15	Temperature control references (TCR's)
16–17	Black plates
18	Cone radiometer facing down

The test results are plotted in Figs. 5 and 6. These graphs compare the measured intensity of each device to that measured by Cone 8 (TCM cone). Two discrepancies are apparent. A departure of the ratio from 1.00 indicates a difference in absolute intensity; a nonhorizontal line indicates a difference in intensity ratio at various intensity levels. The results plotted in Fig. 6 were deduced from simple temperature measurement devices. Except for the cone radiometers, Fig. 5 presents results for commercially available instruments.

Fig. 6 shows good agreement among all test items (excluding the cone) except at low intensities. The high data at low intensities is unexplained, but it appears to be associated with low temperature.

The lower thermal shield data was in considerably better agreement with Cone 8 during this test than during the TCM test. There was scatter in shield temperatures for the TCM test at 125 w/ft² intensity. This fact, combined with the agreement among plates, TCR's, and the shield in the comparison test, suggests that the comparison test data are the more reliable. It was concluded that the TCM test levels as measured by the cone were substantially correct. The cone radiometer will therefore be used to set intensity levels for the flight spacecraft tests.

6. Venus Encounter Thermal Heating

An analysis has been performed which determines the worst-case thermal effect of the planet Venus on the *Mariner* Venus 67 spacecraft during encounter. As the spacecraft passes by the planet Venus, it is subjected to two incident heat fluxes in addition to the direct solar flux. These fluxes are: (1) solar energy reflected from the planet (primarily from the Venusian atmosphere), and (2) longer wavelength energy radiated from the Venusian atmosphere and surface (commonly referred to as "planetshine").

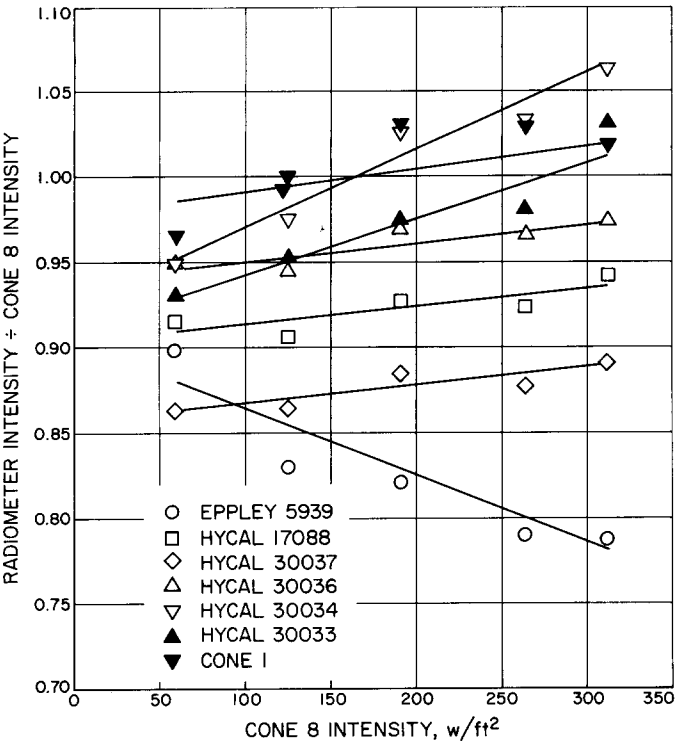

Fig. 5. Radiometer relative intensity comparison test

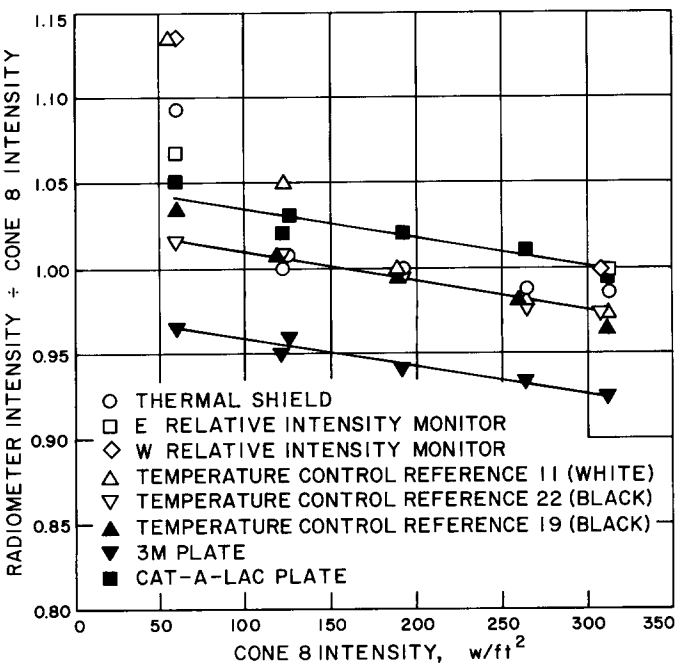

Fig. 6. Temperature measurement items, relative intensity comparison test

CONFIDENTIAL
UNCLASSIFIED

UNCLASSIFIED
CONFIDENTIAL

The Lockheed heat flux program was utilized to determine the reflected solar and planetshine inputs to the spacecraft for various points in the flyby trajectory. For the purpose of this analysis, the blackbody temperature of the planet was considered uniform at −5°F, and the solar reflectance (albedo) was taken to be 80%. The flyby trajectory which corresponds to a launch date of June 17, 1967, was used because its nominal point of closest approach is nearer to the planet than that of any other launch date. The use of this trajectory assures a conservative analysis, since the planet fluxes vary inversely with the square of the distance from the planet.

Once the absorbed flux versus time relationships were determined for various surfaces of the spacecraft, they were plugged into the thermal analyzer computer program which utilized a nodal representation of the spacecraft to translate flux-time relationships into temperature-time data. The final results are plotted in Figs. 7 and 8 in terms of deviation from Venus cruise temperature (ΔT) versus time from encounter. The results as presented are for a worst-heating case. The temperature rises seen during the actual encounter will be somewhat less than those shown on the accompanying plots.

The analysis is set up so that it can be repeated without difficulty once the correct trajectory parameters are available (i.e., after midcourse maneuver). At that time, it will be possible to update the expected temperature variations so that they apply more closely to the real case instead of simply bracketing it.

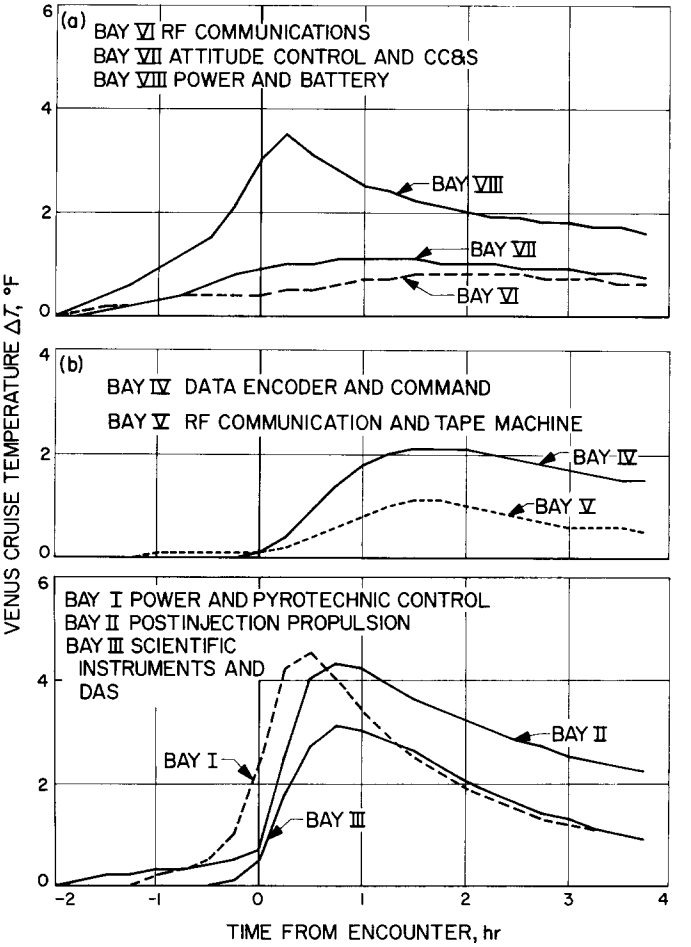

Fig. 7. Effect of Venus on average bay temperatures

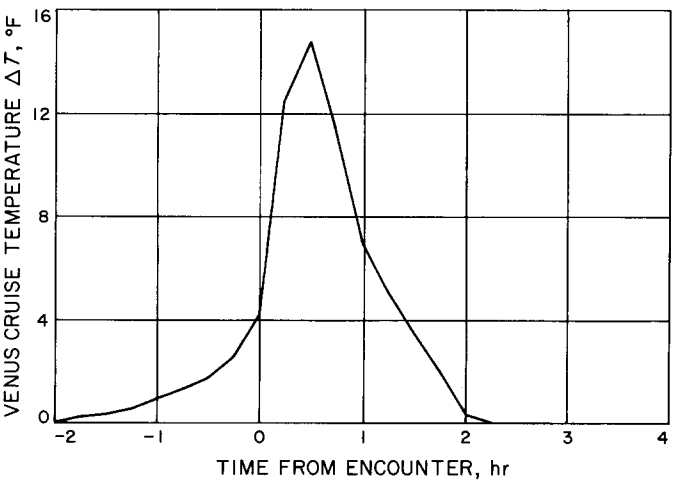

Fig. 8. Effect of Venus on solar panel temperatures

E. Guidance and Control

1. Midcourse Guidance Error Analysis

a. Introduction. The normal sequence followed during an unmanned interplanetary flight, such as the *Mariner* Venus 67 mission, requires the execution of one or more midcourse maneuvers. These maneuvers are required to correct for the initial injection errors so that the spacecraft will arrive at the target planet within an acceptable region around the desired arrival point.

The magnitude and direction of the midcourse maneuver is a function of the estimated trajectory, as determined by radio tracking, and the deviation between the estimated arrival point and the desired arrival point. The deviations arising in the execution of the midcourse maneuver, coupled with the uncertainty in determining the actual trajectory, will cause a residual miss at the target planet. This article will be concerned only with the residual miss caused by the execution uncertainties in the midcourse maneuver.

UNCLASSIFIED
CONFIDENTIAL

UNCLASSIFIED

The component source errors which arise during the execution of the midcourse maneuver result in an actual velocity increment vector which deviates from the desired velocity increment vector in orientation and magnitude. These deviations in the desired velocity increment vector cause the resultant residual miss at the target planet.

The target miss parameters, $\mathbf{B}\cdot\mathbf{T}$, $\mathbf{B}\cdot\mathbf{R}$, and T_f represent respectively: the projection of the hyperbolic impact parameter, **B** (the vector lying in the plane of the trajectory from the center of the target planet perpendicular to the incoming asymptote of the hyperbolic trajectory) on the coordinate axis **T**; the projection of the impact parameter **B**, on the coordinate axis **R**; and the time of flight T_f. The vectors **T** and **R** form two axes of a right-handed coordinate system, $\mathbf{R} = \mathbf{S} \times \mathbf{T}$, where **S** is a unit vector in the direction of the incoming asymptote, **T** a unit vector perpendicular to **S** that lies in a fixed plane such as the equatorial plane, and **R** is a unit vector completing the right-handed coordinate system. Ref. 1 gives a discussion of the target miss parameters.

The results of the midcourse guidance error analysis study are expressed in terms of: (1) the variances of the total miss parameter, $[(\mathbf{B}\cdot\mathbf{R})^2 + (\mathbf{B}\cdot\mathbf{T})^2]^{1/2}$, and the time of flight, and (2) the standard deviations, σ_p, σ_s, and σ_r, associated with the maneuver velocity vector. The quantities, σ_p, σ_s, and σ_r, are, respectively,

(1) the standard deviation of the pointing error (directional deviation in the maneuver velocity vector)

(2) the standard deviation of the proportional error (deviation in the velocity vector proportional to the magnitude of the velocity vector)

(3) the standard deviation of the resolution error (a deviation in the magnitude of the velocity vector not dependent on the magnitude of the vector)

The *Mariner* Venus 67 midcourse guidance accuracy study was basically the same as that for the *Mariner* Mars 1964 mission, with the replacement of Mars with Venus as the target planet. The component error sources used for *Mariner* Venus were unchanged from those used for *Mariner* Mars 1964. For the techniques employed in this analysis, refer to the comprehensive coverage of the midcourse guidance analysis in SPS 37-24, Vol. II, pp. 30–42.

b. Results of Mariner Venus 67 midcourse guidance analysis study. The results of the *Mariner* Venus 67 midcourse guidance error analysis were based on a launch date of June 17, 1967, and a midcourse maneuver June 22, 1967. The midcourse maneuver component error sources considered and the 1-σ values of each are listed in Table 1.

The statistical investigation of the miss parameter deviations as a function of the midcourse component errors was conducted using a Monte Carlo analysis and computer program (SPS 37-24, Vol. II). The Monte Carlo Program randomly selects possible midcourse maneuvers from a Gaussian distribution with covariance Λ_v (the covariance matrix of maneuvers necessary to correct the random residuals due to injection uncertainties), and calculates the pitch and roll turns required to execute each maneuver. The deviation in each maneuver velocity vector selected is calculated, based upon random selections of the component error source magnitudes. This error in the thrust vector is mapped to the target planet in terms of a residual miss for each maneuver selected. A statistical estimate of the variance of each miss parameter is calculated, based upon all the random maneuvers selected. Thus, the variance of the total miss parameter, $[(\mathbf{B}\cdot\mathbf{T})^2 + (\mathbf{B}\cdot\mathbf{R}^2]^{1/2}$, and the variance of the time of flight, T_f, are found for each component error source.

The results of the Monte Carlo study are given in Table 1 in terms of the individual component errors which are divided into groups contributing to the pointing, proportional, and resolution errors in the thrust vector.

For each component error source, Table 1 gives:

(1) the 1-σ standard deviation of the error source

(2) the type of distribution (Gaussian or uniform) assumed for the error source

(3) the variance of the total miss parameter, $[(\mathbf{B}\cdot\mathbf{R})^2 + (\mathbf{B}\cdot\mathbf{T})^2]^{1/2}$

(4) the variance of the time of flight, T_f

Taking the root square of the component errors used in the Monte Carlo Program, the 1-σ standard deviations σ_r and σ_s were calculated to be:

σ_r = 1-σ resolution error = 0.0626 m/sec

σ_s = 1-σ proportional error = 0.00760

The 1-σ pointing error is represented in Figs. 9–11 as a function of the maneuver pitch and roll magnitudes expressed in degrees. The pointing error may be expressed in terms of components parallel to two orthogonal axes normal to the thrust vector.

UNCLASSIFIED

UNCLASSIFIED
CONFIDENTIAL

Table 1. Monte Carlo Program study results

I. Sources of pointing errors	1-σ standard deviation	Type of error source distribution	Variance of total miss, km^2	Variance of time of flight, sec^2
1. Roll gyro drift	1.61E-6[a] rad/sec	Gaussian	1.73E5	2.74E5
2. Yaw gyro drift	1.61E-6 rad/sec	Gaussian	5.12E4	4.49E4
3. Pitch gyro drift	1.61E-6 rad/sec	Gaussian	7.55E4	6.03E4
4. Misalignment of the yaw gyro with the pitch axis				
a) A/C[b] internal to case	1.73E-3 rad	Gaussian	4.89E4	6.60E4
b) structural misalignment of case to the primary reference plane	0			
c) structural misalignment of case to the secondary reference plane	0			
5. Misalignment of roll gyro with pitch axis				
a) A/C internal case	1.73E-3 rad	Gaussian	2.89E4	2.79E4
b) structural misalignment of case to the primary reference plane	0.29E-3 rad	Gaussian	8.11E2	7.83E2
c) structural misalignment of case to the secondary reference plane	0.144E-3 rad	Gaussian	2.00E2	1.93E2
6. Misalignment of pitch gyro with roll axis				
a) A/C internal to case	1.73E-3 rad	Gaussian	3.76E4	2.75E4
b) structural misalignment of case to the primary reference plane	0.29E-3 rad	Gaussian	1.06E3	7.74E2
c) structural misalignment of case to the secondary reference plane	0.14E-3 rad	Gaussian	2.60E2	1.91E2
7. Misalignment of yaw gyro with roll axis				
a) A/C internal to case	1.73-3 rad	Gaussian	4.35E4	3.45E4
b) structural misalignment of case to the primary reference plane	0.29E-3 rad	Gaussian	1.22E3	9.69E2
c) structural misalignment of case to secondary reference plane	0.144E-3 rad	Gaussian	3.01E2	2.39E2
8. Roll limit cycle size	2.4E-3 rad	Uniform	6.55E4	1.01E5
9. Roll sensor null offset (electrical–mechanical)	4.63E-3 rad	Gaussian	2.34E5	3.61E5
10. Roll switching amplifier null offset	0.57E-3 rad	Gaussian	3.54E3	5.46E3
11. Roll sensor structural misalignment	0.29E-3 rad	Gaussian	9.18E2	1.41E3
12. Yaw limit cycle size	4.9E-3 rad	Uniform	1.39E5	1.31E5
13. Yaw Sun sensor null offset (electrical–mechanical)	3.18E-3 rad	Gaussian	5.88E4	5.56E4
14. Yaw switching amplifier null offset	0.57E-3 rad	Gaussian	1.88E3	1.77E3
15. Yaw Sun sensor structural misalignment	0.80E-3 rad	Gaussian	3.72E3	3.52E3
16. Pitch limit cycle size	4.9E-3 rad	Uniform	1.86E5	1.46E5
17. Pitch Sun sensor null offset (electrical–mechanical)	3.18E-3 rad	Gaussian	7.88E4	6.20E4
18. Pitch sensor structural misalignment	0.80E-3 rad	Gaussian	4.99E3	3.93E3
19. Pitch switching amplifier null offset	0.57E-3 rad	Gaussian	2.51E3	1.98E3
20. CC&S[c] pitch turn time resolution	0.29 sec.	Uniform	6.42E3	5.05E3
21. Pitch capacitor leakage	5.20E-3 rad	Uniform	2.09E5	1.65E5
22. Pitch rate calibration	4.4E-6	Gaussian	4.86E4	5.25E4
23. CC&S roll turn time resolution	0.29 sec	Uniform	9.57E3	1.51E4
24. Roll capacitor leakage	5.20E-3	Uniform	3.12E5	4.91E5
25. Roll rate calibration	4.4E-6 rad/sec	Gaussian	8.11E4	1.20E5

[a]1.61E-6: 1.61×10^{-6} likewise for other numerical entries
[b]A/C: attitude control
[c]CC&S: central computer and sequencer

CONFIDENTIAL
UNCLASSIFIED

UNCLASSIFIED
CONFIDENTIAL

Table 1. Monte Carlo Program study results (contd)

I. Sources of pointing errors	1-σ standard deviation	Type of error source distribution	Variance of total miss, km^2	Variance of time of flight, sec^2
26. Motor and center-of-mass misalignments				
a) angle between undeflected thrust vector and rocket engine centerline at nozzle	0.825E-3 rad	Gaussian	6.27E2	5.44E2
b) perpendicularity of rocket engine mounting flange to rocket engine centerline	2.04E-4 rad	Gaussian	9.61	15.0
c) parallelism of rocket engine mounting surface to thrust plate mounting pads	3.27E-4 rad	Gaussian	32.7	50.1
d) offset mounting of rocket engine in the thrust plate	3.04E-3 in.	Gaussian	2.19E2	2.43E2
e) PIPS[d] reference plane inclined to PIPS support structure mounting surface on the octagon structure	2.89E-4 rad	Gaussian	0.470	0.728
f) line in PIPS reference plane parallel to primary reference plane, is parallel to PIPS support structure mounting surface on octagon structure	2.89E-4 rad	Gaussian	12.5	20.0
g) concentricity of the rocket engine mounting hole to the thrust plate mounting holes for substructure	2.86E-3 in.	Gaussian	4.31E2	4.78E2
h) concentricity of thrust plate substructure mounting holes	2.07E-3 in.	Gaussian	2.26E2	2.50E2
i) concentricity of substructure/octagon structure mounting holes	3.04E-3 in.	Gaussian	2.19E2	2.43E2
j) uncertainty in position of center of gravity	2.90E-2 in.	Gaussian	4.34E4	4.81E4
27. Roll autopilot jet vane actuator				
a) mechanical–electrical null offset	1.01E-3 rad	Gaussian	1.16E3	1.83E3
b) amplifier null offset	2.53E-3 rad	Gaussian	7.29E3	1.15E4
28. Yaw autopilot jet vane actuator				
a) mechanical–electrical null offset	1.01E-3 rad	Gaussian	3.35E3	2.64E3
b) amplifier null offset	2.53E-3 rad	Gaussian	2.11E4	1.66E4
Total effect of pointing error (variance)			1.987E6	2.344E6
Total effect of pointing error (1-σ standard deviation)			1.410E3 km	1.531E3 sec

II. Proportional errors	1-σ standard deviation	Type of error source distribution	Variance of total miss, km^2	Variance of time of flight, sec^2
1. Propulsion system errors	0.374 lb_f	Gaussian	3.47E5	3.53E5
2. Initial mass error	0.462 lb_m	Gaussian	4.46E3	4.54E3
Total effect of proportional error (variance)			3.51E5	3.58E5
Total effect of proportional error (1-σ standard deviation)			5.92E2 km	5.98E2 sec

III. Resolution errors	1-σ standard deviation	Type of error source distribution	Variance of total miss, km^2	Variance of time of flight, sec^2
1. Propulsion system resolution errors	0.464 lb_f sec	Gaussian	1.37E3	1.44E3
2. CC&S burn time resolution	1.71E-2 sec	Uniform	4.68E3	4.90E3
3. CC&S command delay error	1.16E-3 sec	Gaussian	0.215E2	0.226E3
4. Pressure transient error	2.23 lb_f sec	Gaussian	3.16E4	3.31E4
5. Drag impulse error	2.50 lb_f sec	Gaussian	3.98E4	4.17E4
Total effect of resolution error (variance)			7.747E4	8.116E4
Total effect of resolution error (1-σ standard deviation)			2.783E2 km	2.849E2 sec
Total effect of execution error (variance)			2.415E6	2.425E6
Total effect of execution error (1-σ standard deviation)			1.554E3 km	1.557E3 sec

[d]PIPS: post-injection propulsion subsystem

UNCLASSIFIED
CONFIDENTIAL

UNCLASSIFIED
CONFIDENTIAL

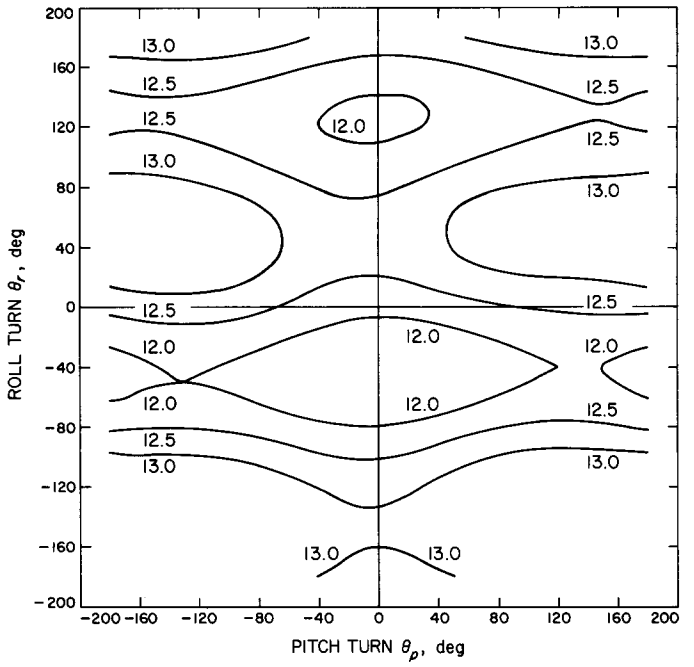

Fig. 9. Contours of constant total pointing error (milliradians)

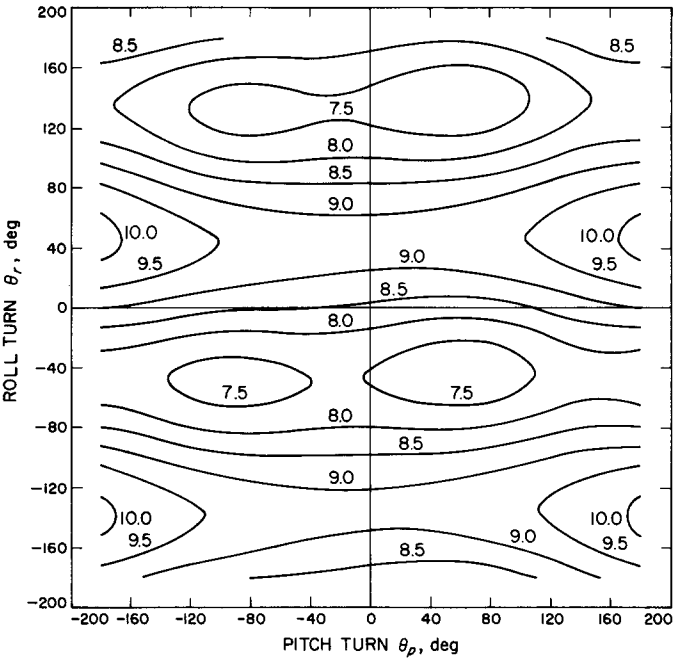

Fig. 11. Contours of constant pointing error motor yaw axis component (milliradians)

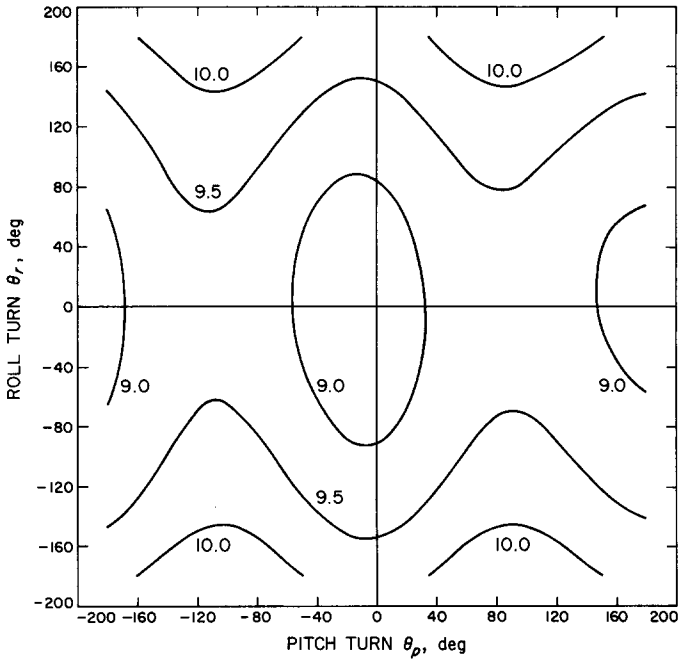

Fig. 10. Contours of constant pointing error motor roll axis component (milliradians)

Figs. 10 and 11 represent the standard deviation of the error component along the two axes normal to the thrust vector (called motor yaw and roll). Fig. 11 represents the total pointing error, which is defined to be the rms of the component errors along each axis.

A second statistical computer program was used to map the standard deviations (derived above) in the maneuver velocity vector into a dispersion ellipse in the **R-T** plane at the target planet. This program, called the four-parameter guidance analysis program (Ref. 2) uses the same mapping matrices as does the Monte Carlo Program. It differs from the Monte Carlo Program, however, in that it does not use a random selection of maneuvers and component errors to establish the statistics, but utilizes the input standard deviations in place of the sampling techniques of the Monte Carlo Program.

The four-parameter program assumes a circular normal distribution with zero correlation between the errors normal to the thrust vector, thus requiring the standard deviations with respect to each axis to be equal. The Monte Carlo Program only requires that the component source errors be uncorrelated and Gaussian.

From the covariance matrix of the residual miss computed in the Monte Carlo Program, the dispersion ellipse in the **R-T** plane may be found. Curve A in Fig. 12 represents the Monte Carlo dispersion ellipse. Curves B and C represent the dispersion ellipses calculated by the four-parameter program for two sets of the thrust vector

CONFIDENTIAL
UNCLASSIFIED

UNCLASSIFIED

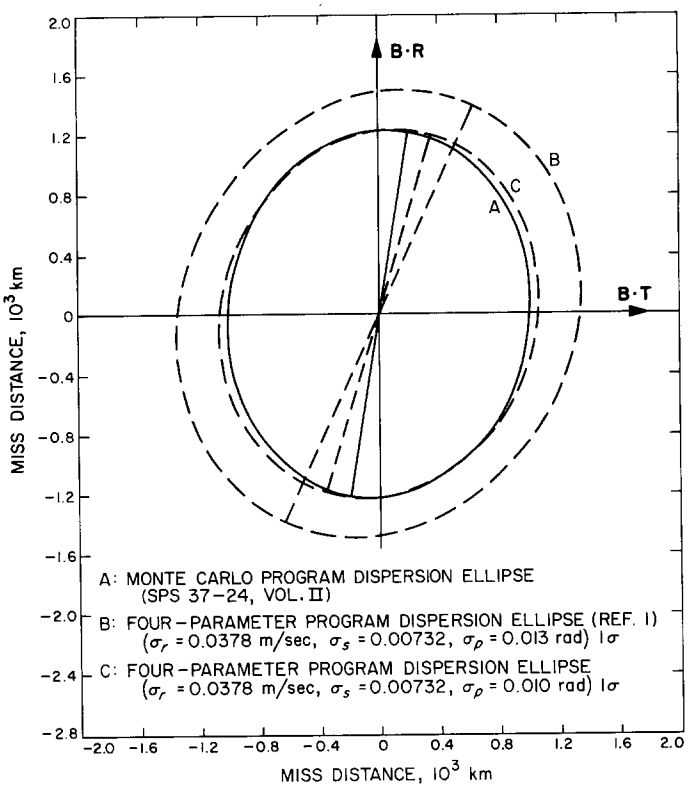
B·R
B·T
A
B
C
MISS DISTANCE, 10^3 km
MISS DISTANCE, 10^3 km
A: MONTE CARLO PROGRAM DISPERSION ELLIPSE (SPS 37-24, VOL. II)
B: FOUR-PARAMETER PROGRAM DISPERSION ELLIPSE (REF. 1) (σ_r = 0.0378 m/sec, σ_s = 0.00732, σ_p = 0.013 rad) 1σ
C: FOUR-PARAMETER PROGRAM DISPERSION ELLIPSE (σ_r = 0.0378 m/sec, σ_s = 0.00732, σ_p = 0.010 rad) 1σ

Fig. 12. Target planet dispersion ellipses (1 σ)

standard deviations, i.e., σ_p, σ_s and σ_r. Curve C in Fig. 12 shows that there is a combination of σ_p, σ_s and σ_r which can be processed by the four-parameter program to yield a dispersion ellipse that closely approximates the dispersion ellipse calculated from the Monte Carlo Program.

The set that gives the closest approximation is:

σ_r = 1-σ resolution error = 0.0622 m/sec

σ_s = 1-σ proportional error = 0.00838

σ_p = 1-σ pointing error = 0.00911 rad/axis or 0.0129 rad pointing error.

Comparing the above set of standard deviations with that set calculated using the component errors listed in Table 1, it is found that the value 0.0129 rad total pointing error agrees favorably with the range of values shown in Fig. 9. The 12% difference in the velocity magnitude error is almost entirely due to the difference between the two proportional errors. This difference is reasonable when the two computer programs are compared, as discussed below.

The four-parameter program assumes that the distribution of the pointing error about the velocity vector is normal and circular and has no preferred orientation. The Monte Carlo Program is not constrained by this assumption; in fact, it is biased toward certain orientations, since certain pitch and roll rotations are forbidden by the constraint that the Earth must remain within the radio low-gain antenna pattern during the maneuver. The circular assumption of the four-parameter program (the standard deviation per axis is equal), in conjunction with the radio low-gain orientation constraint of the Monte Carlo Program, increases the probability that the orientations of the dispersion ellipses will be different. This statistical difference between the two programs causes the differences between the two sets of thrust vector standard deviations.

In reference to Table 1, it is noticed that with respect to the component error source contributions to the thrust vector pointing error, the major contributors are the gyro drifts (particularly roll drift), roll sensor null offset, the limit cycle size, and capacitor leakage. The roll capacitor leakage is the major single contributor to pointing accuracy.

The propulsion system proportional errors are the major contribution to velocity magnitude accuracy; in fact, they dominate all other contributors to velocity magnitude accuracy.

2. Attitude Control Subsystem

The process of modifying and qualifying for flight the hardware which constitutes the attitude control subsystem for the *Mariner* Venus 67 spacecraft has, for the most part, progressed smoothly. There have been some delays; e.g., the zener diodes that were to be added to the electronics unit were found to have one lead unweldable by the techniques used in the construction of the unit. Consequently, a new welding process was developed on the Laboratory, and the units successfully modified by Laboratory personnel. Also, a voltage level change in the pyrotechnics subsystem interface with the terminator sensor forced a redesign of the simple two-transistor electronic circuit of this unit, with subsequent delays in fabrication and testing. At this time, however, the M67-1 spacecraft has been assembled and is undergoing system-type testing; it is soon to be moved to the environmental facility, and the M67-2 spacecraft is currently being assembled.

The attitude control subsystem has performed nominally during all of the tests planned; the gyro control assembly was subjected to an unplanned test wherein

UNCLASSIFIED

UNCLASSIFIED

the gyros were given input rates in excess of those specified. A complete retest of the assembly in the inertial sensors laboratory failed to reveal any degradation or change in performance characteristics. The attitude control gas system was also inadvertently subjected to a rather severe test: it was almost completely drained of nitrogen. Retesting revealed that the pressure regulator's characteristic pressure drop had changed slightly, but was still within specification.

During qualification testing, a spacecraft reflectance test was performed to verify the compatibility of the spacecraft and the optical sensors. The testing was done in the Optical Sensor Group's Celestarium, and involved mounting the spacecraft (in this instance, the temperature control model) in various attitudes within a 28-in.-diameter "sun bundle" (i.e., a column of sunlight) and measuring the incident and reflected light at the various sensor locations. The results of this test indicated that each sensor had a sufficient "margin of safety" to spacecraft reflected light. A significant development in testing was the fabrication of a stray light simulator for testing the Canopus sensor's reaction to stray light. This device is designed to simulate stray light in space, and to permit evaluation of the effects of stray light on the Canopus sensor. Modifications to extend its use to other sensors are possible. A detailed report on the simulator will be the subject of a future article.

One continuing problem has been the apparent loss of torque gain (output torque versus input current) of the jet vane actuators. These units are the same as those used on *Mariner* Mars 1964, and are actually spares from that program. As indicated in the SPS 37-42, Vol. II, the only modification to these units has been the substitution of DC-11 for Apezione-N as the shaft seal lubricant.

The actuators for the first spacecraft eventually passed all flight qualification tests, as did the actuators for the second. However, after one flight-acceptance vibration test, the M67-2 actuators were observed to have dropped below the torque gain specification lower limit. Investigation of the procedure and equipment used to remagnetize the rotor of these DC torquers showed that the machine used in the remagnetization process did not have the field strength originally, specified by the actuators' designers. After remagnetization with a machine of approximately double the field intensity, the actuators passed the flight-qualification testing. However, since the M67-1 actuators were remagnetized with the weaker machine, they were now suspect, and arrangements were made to measure the torque gain of these units in the Spacecraft Assembly Facility (SAF); they had already been installed on the M67-1 spacecraft. This test revealed that the torque gain of these actuators had also degraded below actuator specifications. At this time, the M67-2 actuators, which by now had been delivered to SAF and were in bonded storage, were remeasured and found to be degraded. Since the only activity involving these actuators between the measuring of an in-spec torque gain and an out-of-spec torque gain had been an attitude control subsystem integration test, the portions of this test involving the jet vane actuators was rerun. This test is a verification that the electronics unit, the gyro control assembly, the Canopus sensor, the gas system and the jet vane actuators interface properly and work together as they should. The results of this retest were inconclusive, and the current status of the problem is that at this time, the causes and reason for the degradation in torque gain are unknown. Three areas of investigation are being pursued: (1) magnetic stability of the actuator rotor as a function of stabilizing and operating stator current levels; (2) the possibility that large transient currents are being generated by the collapsing magnetic field of the stator; and (3) the possibility of an incompatibility between either the test equipment used or the autopilot and the actuator, so that large, destabilizing currents can exist in the actuator stator.

3. Planet Sensor

a. Background. In March 1966, the design of the planet sensor was initiated (SPS 37-39, Vol. II). The operational objective of the sensor (Figs. 13 and 14) was to sense the illuminated limb of Venus and initiate the spacecraft encounter sequence. The planet sensor output (PSO), backed up by an onboard timer, would provide a start signal approximately 1 hr before planet encounter.

The narrow-angle Mars gate (NAMG), SPS 37-25, Vol. VI, p. 15, flown on *Mariner* Mars 1964 was to be utilized with as little modification as necessary. The following general requirements were designated:

(1) Fixed pointing angle and field of view (FOV).

(2) The angle and FOV were to be selected on the basis of providing a PSO at a minimum of 38 min before encounter and a minimum PSO time dispersion, relative to encounter, for any of the planned combinations of trajectories and launch dates. Timing was also to be optimized relative to midocculta-tion as a secondary consideration.

UNCLASSIFIED

UNCLASSIFIED
CONFIDENTIAL

Fig. 13. Planet sensor

(3) The unit must have a high stray light rejection, since preliminary estimates placed the pointing angle near the Sun.

(4) The unit should interface with existing data automation subsystem (DAS) excitation (+ 20 v dc at ≤5 ma), and the PSO should operate directly into existing DAS logic inputs.

In addition, a search was to be made for a suitable spacecraft location. An area near the Canopus sensor was considered primarily and was ultimately selected.

b. Planet sensor design. The following preliminary design steps were required before a prototype could be assembled and tested.

PSO timing. Determination of the optimum field-of-view with consideration to previously outlined requirements was undertaken. This was primarily accomplished by hand drawn plots of the illuminated limb of Venus. The plots, as in Fig. 15, were drawn for each 3 min of flight in the vicinity of encounter minus 1 hr, and for each of five points (limits and center) in the 3σ trajectory dispersion pattern. This was repeated for the total span

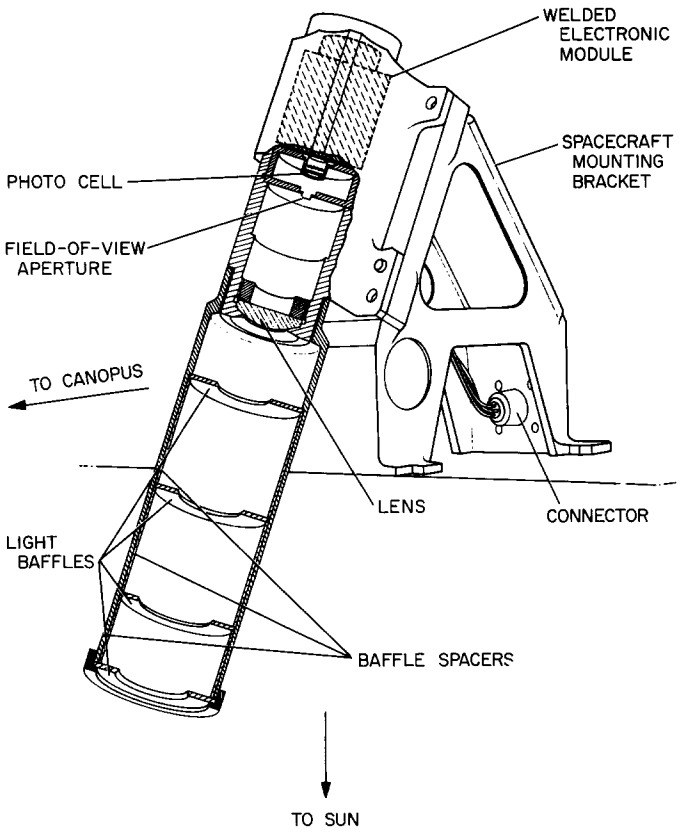

Fig. 14. Cutaway planet sensor

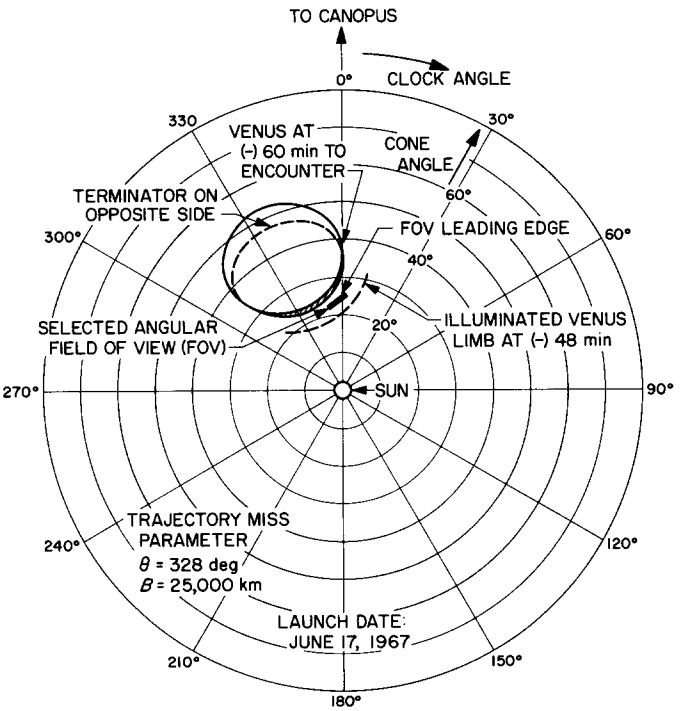

Fig. 15. Planet sensor field of view superimposed at −2 min from contact with illuminated limb of Venus

UNCLASSIFIED
CONFIDENTIAL

UNCLASSIFIED

of launch dates from June 12–27. As a result of these graphical iterations, a "leading edge"[1] for the FOV was selected. A computer program was modified to determine contact time of the illuminated limb with the leading edge of the FOV, and the results, which were in agreement with graphically tabulated data, are:

PSO relative to encounter $= 60^{+12}_{-13}$ min

PSO relative to midoccultation $= 60^{-8}_{+16}$ min

PSO relative to enter–exit occultation $= 60^{-18}_{+40}$ min

The next step was to determine the angular width of the field back of this leading edge. This width would have little effect on timing, but was controlled by the conflicting considerations of viewing as much of the planet as possible (to keep the light level threshold maximized) and limiting the stray light susceptibility. Based on these considerations, the angular width was optimized at 1°30'.

Light level threshold. Determination of optimum light level threshold to achieve PSO was next accomplished. The trajectory which placed the planet sensor FOV nearest to the illuminated horns of Venus (Fig. 15) was chosen as worst case (i.e., lowest illumination). An overlay of the selected FOV onto a calculated intensity map of this sector provided a conservative value of 0.07 ft-c to the detector. This included the effects of effective lens aperture, detector spectral response, and a conservative calculation of Venus' spectral irradiance and intensity. The threshold, for PSO, was then set at 0.01 ft-c, which provides a safety factor of 7. A larger safety factor was considered undesirable because of increased susceptibility to stray light, and a less stable control of threshold point. The stability decreases at the lower light levels due to the characteristics of the CdS detector, and the electronics module "seeing" a higher (dark) impedance.

Location. Optimum location was next determined. A prime area near the Canopus sensor was available. This afforded the clearest view into the desired direction since the 0° clock angle of Canopus coincided with the planet sensor clock angle axis, and stray light sources were already minimized for the Canopus sensor. The other choices afforded less shading from the Sun and spacecraft stray light sources, or less space for orientation of the sensor baffle tube. A further consideration, at the time, involved a possible change in trajectories. This may have required repositioning of the sighting angle which could be accomplished in the selected area.

Light baffles. Planet sensor stray light baffles were next designed on the basis of maximum stray light rejection consistent with simplicity of design and the shroud clearance which limited the light baffle tube length. The baffle's (Fig. 16) were carefully machined, liquid honed and anodized to provide effective light trapping and a minimum of scattering by virtue of their sharp edges.

Detector and electronics module. In parallel with the optical–mechanical considerations, a test program on the cadmium sulfide (CdS) detector and electronics module was conducted. 100 Clairex CL705L CdS photo conductive cells from the same production run were obtained; 50 of these passed a preliminary visual examination and were selected for screening. After all screening tests, five were deemed suitable for the planet sensor, i.e., they had consistent high dark resistance, a similar resistance versus light level, and the least deviation of characteristics during screening. The selected CdS cells also exhibited a negative 15% temperature characteristic at the desired threshold level.

The electronics module under test demonstrated a compensating positive temperature characteristic with the

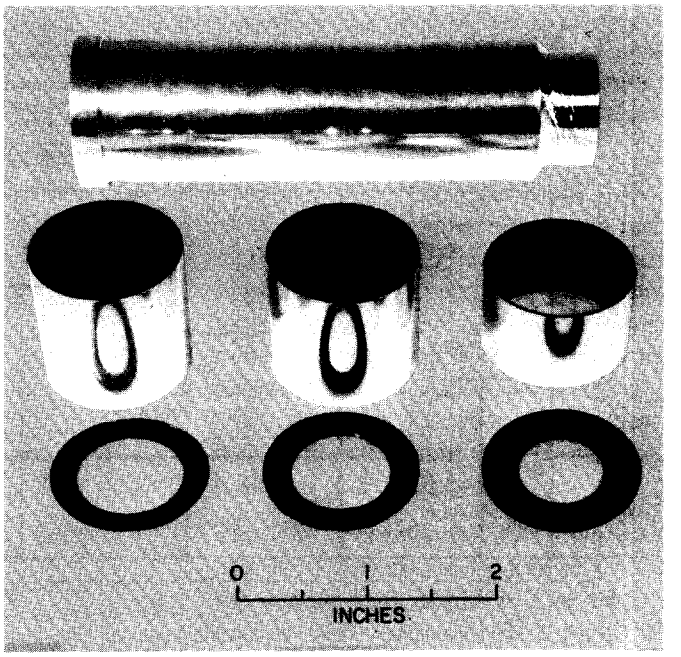

Fig. 16. Light shade assembly

[1]Leading edge is defined by a line (41°4' away from 0° clock angle that is 4°33' in length) which first intercepts the planet limb. This is identified in Fig. 15.

UNCLASSIFIED

UNCLASSIFIED
CONFIDENTIAL

result that the combination of CdS cell and electronics provided a constant light level threshold over the environmental type-approval (TA) temperature range. The final circuit, as shown in Fig. 17, being arranged in the form of a bridge, also compensated for ± 20% excitation voltage change and up to 50% ripple on the excitation line. Provision is made to adjust the light level threshold of the module after encapsulation by addition of an external shunting resistor (RX).

The circuit functions similarly to a Schmitt trigger. When the CL705L CdS photoconductive cell is illuminated sufficiently to cause the voltage on the base of Q1 to exceed its reverse bias, both transistors switch state. The collector potential of the output transistor Q2, which is now in the *off* state, rises to approximately 9 v. The switching time, after threshold, is less than 10 msec. Filtering on the base of Q1, the excitation load line, and the PSO load line provide a low noise susceptibility. Additionally, the DAS input is reverse biased 5 times the normal "no planet" output voltage.

c. Development. In early August 1966, a prototype planet sensor was assembled and subjected to extensive type-approval testing. During TA vibration, the sensor was inadvertantly exposed to a level 20 to 50 times normal vibration level. The unit was then functionally tested and showed no change in performance. It was then completely disassembled, inspected, and reassembled. The prototype was redesignated as the TA unit (S/N 001) and passed all TA tests. Two more units were fabricated, tested, and delivered to the M67-1 and M67-2 spacecrafts in late August and December 1966, respectively. During the interim, an intensive test program subjected the CdS cells and spare welded modules to a wide range of long-term extremes in environmental conditions. As a result, the stability of the CdS cells and electronics were encouraging in establishing long-term reliability.

A measured survey of stray light sources from the Sun shade, Bay VIII thermal louvers and solar panels, etc., established a probable 200 ft-c maximum intensity, no closer than 9 deg from the mean planet sensor optical axis. Measured performance of the planet sensor indicated the unit could reject in excess of 30,000 ft-c, 8.5 deg off axis, thereby assuring proper operation even if the Sun shade should not deploy. A plot of the stray light rejection characteristics is shown in Fig. 18. Each "constant intensity contour" represents the intensity required to cause PSO, or the intensity required at that angle to allow the equivalent of 0.04 ft-c to fall on the CdS detector (lens to detector gain = ×4).

d. Operational support equipment (OSE) hood. The OSE hood was designed as an aid to environmental testing, but primarily for spacecraft subsystem checkout. The principal configuration is a closed hood, Fig. 19, that fits over the entrance aperture of the planet sensor to the exclusion of all other light. It consists of a miniature

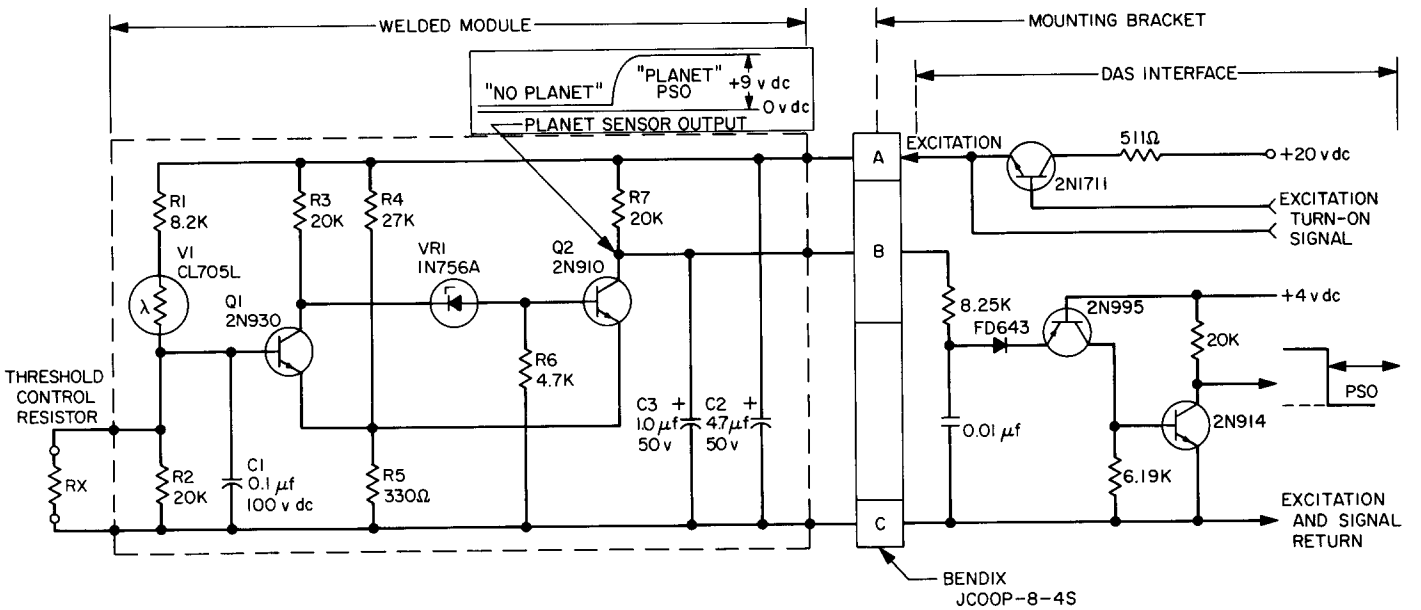

Fig. 17. Planet sensor schematic

CONFIDENTIAL
UNCLASSIFIED

UNCLASSIFIED
CONFIDENTIAL

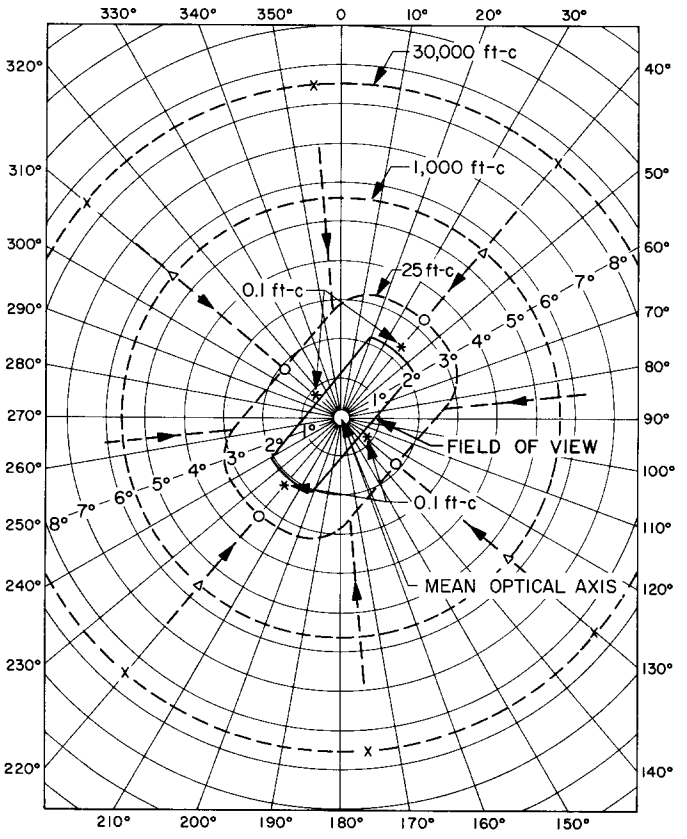

Fig. 18. Planet sensor stray light rejection

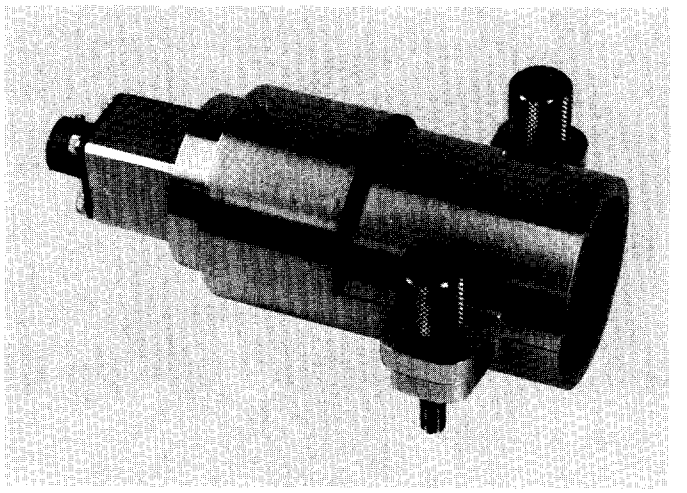

Fig. 19. Operational support equipment hood

lamp (Chicago miniature lamp CM8-870), with a diffused surface placed behind a partially transmitting and diffusing Teflon screen. This screen provides an even surface brightness of approximately 0.5 ft-L at the required planet sensor threshold level and is large enough so that alignment is not critical.

For testing in an environmental chamber, the lamp is supplied a variable current. This is monitored during test to ascertain changes in threshold by noting changes in lamp current required to cause PSO. For spacecraft checkout, the lamp will operate (on OSE command) at a current sufficient to provide three times planet sensor threshold. Each OSE hood is serialized and mated to a particular planet sensor.

Table 2. *Mariner* Venus 67 planet sensor characteristics

Weight	257 g
Power	42 mw (20 v dc at 2.1 ma)
Electronics (welded module)	2 transistors, 1 zener diode, 8 resistors, 3 capacitors, 1 CdS photoconductive cell
Dimensions	Maximum length: 8 in. Maximum dimensions ⊥ to this: 6.25 in.
Spacecraft pointing angle	Plane of constant clock angle equal to zero and 24°54′ away from Sun
Field of view	4°33′ × 1°30′ (clear field assured by front light baffles 6° circular)
Lens	Single element plano convex crown glass
Detector	Cadmium sulfide, Clairex CL705L (visible)
Stray light rejection	3 × 10⁻⁶ (30,000 ft-c) at 8.5° off axis
Input	Light level threshold: 0.01 ft-c at 5500 Å (peak response)
Output	9-v step to data automation subsystem when input exceeds threshold. Starts Timer B to initiate encounter sequence

e. Functional details. The outline of planet sensor characteristics is given in Table 2. A detailed breakdown of these characteristics follows.

Excitation: 20 v dc ±5% at 5 ma max with 4% peak-to-peak ripple. The maximum current is supplied only if the CdS cell should look directly at the Sun.

Field-of-view: 4°33′ × 1°30′. This is determined by a small rectangular aperture on the focal plane of the lens. The aperture dimensions are closely controlled to minimize light scattering and maintain an accurate FOV. This aperture allows illumination of approximately 50% of the CdS cell active area. The rear view is shown in Fig. 20 and a front view (facing lens) is shown in Fig. 21.

Lens: The lens is optical-quality crown glass, especially selected to be free of scattering strains and bubbles. The edge is ground and coated with a light absorber, and only the central 60% of its diameter is utilized.

UNCLASSIFIED
CONFIDENTIAL

UNCLASSIFIED
CONFIDENTIAL

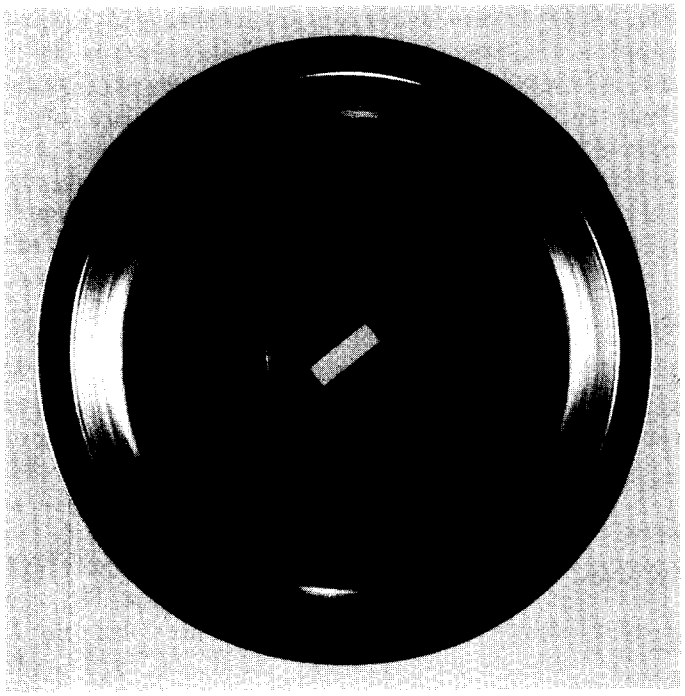

Fig. 20. Aperture

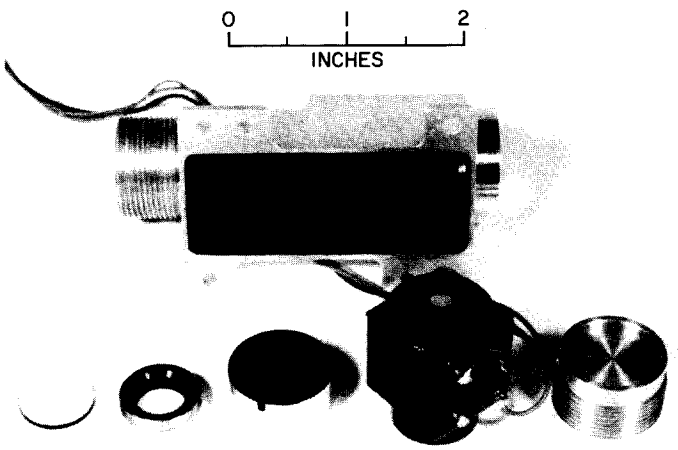

Fig. 21. Planet sensor housing

Housing assembly: In Fig. 21, the lens, lens retainer ring, aperture (front view), welded module (CdS cell facing up), and module retainer plug are shown adjacent to housing into which they are assembled.

Electronics: The unpotted welded module is shown in Fig. 22. The CdS cell is bonded to the face with its sensitive pattern aligned at 41-deg clock angle to match the tilt of the leading edge of the FOV. All components are welded except threshold setting RX, which is added during pre-environmental functional tests. The threshold is set for 0.01 ft-c incident on the planet sensor lens. The lens provides a gain of 4 to the detector. The electronics will reverse state if this threshold intensity is reduced 30% (switch hysteresis). The cell may look directly at Venus Sun without damage (22,000 ft-c) to the CdS cell or electronics. A limiting resistor is placed in series with the CdS cell to limit peak current.

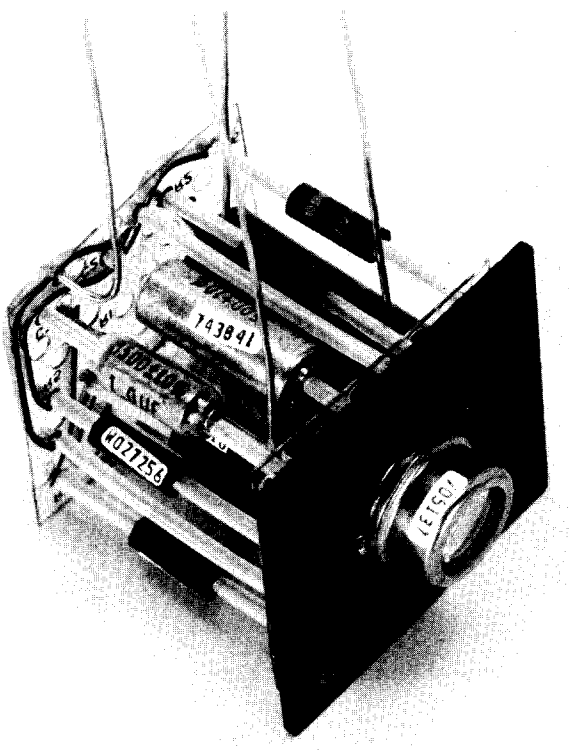

Fig. 22. Welded module

UNCLASSIFIED
CONFIDENTIAL

UNCLASSIFIED
CONFIDENTIAL

References

1. Kizner, W., "A Method of Describing Miss Distances for Lunar and Interplanetary Trajectories," External Publication No. 674, Jet Propulsion Laboratory, Pasadena, California, August 1, 1959.

2. Gates, C. R., "A Simplified Model of Midcourse Maneuver Execution Errors," TR 32-504, Jet Propulsion Laboratory, Pasadena, California, October 15, 1963.

CONFIDENTIAL
UNCLASSIFIED

UNCLASSIFIED
CONFIDENTIAL

III. *Mariner* Mars 1969 Project

A. Introduction

The *Mariner* Mars 1969 Project was initiated in late-December 1965 and formally tasked on February 1, 1966. The primary objective is to conduct two Mars flyby missions in 1969 to make exploratory investigations of the planet which will set the basis for future experiments—particularly those relevant to the search for extraterrestrial life. The secondary objective is to develop the technology needed for succeeding Mars missions.

The spacecraft design concept will be based on the configuration of the successful *Mariner IV* spacecraft, with considerable modifications to meet the 1969 mission requirements and to enhance mission reliability.

The launch vehicle will be the *Atlas/Centaur* SLV-3C. This vehicle, developed under contract for and direction by the Lewis Research Center by General Dynamics/Convair, has a single- or double-burn capability in its second stage and a considerably increased performance rating over the *Atlas D/Agena D* used in the *Mariner IV* mission.

Mariner Mars 1969 missions will be supported by the Eastern Test Range launch facilities at Cape Kennedy, the tracking and data acquisition facilities of the Deep Space Network, and other NASA facilities.

Six planetary-science experiments have been tentatively selected by NASA (subject to integration capability) for the *Mariner* Mars 1969 missions; they are listed in Table 1. Additionally, a planetary-approach-guidance engineering experiment will be incorporated to test the feasibility and flight-readiness of on-board optical sensors and associated data processing techniques necessary for optical approach guidance.

Table 1. *Mariner* Mars 1969 scientific investigations

Experiment	Scientific investigator	Affiliation
Television	R. B. Leighton[a]	California Institute of Technology (CIT)
	B. C. Murray	CIT
	R. P. Sharp	CIT
	N. H. Horowitz	CIT
	J. D. Allen	Jet Propulsion Laboratory (JPL)
	A. G. Herriman	JPL
	L. R. Malling	JPL
	R. K. Sloan	JPL
	N. Davies	Rand Corporation
	C. Leovy	Rand Corporation
Infrared spectrometer	G. C. Pimentel[a]	University of California, Berkeley (UCB)
	K. C. Herr	UCB
Ultraviolet airglow spectrometer	C. A. Barth[a]	University of Colorado
	W. G. Fastie	Johns Hopkins University
Infrared radiometer	G. Neugebauer[a]	CIT
	G. Munch	CIT
	S. C. Chase	Santa Barbara Research Center
S-band occultation	A. J. Kliore[a]	JPL
	D. L. Cain	JPL
	G. S. Levy	JPL
Celestial mechanics	J. D. Anderson[a]	JPL

[a]Principal investigator.

UNCLASSIFIED
CONFIDENTIAL

UNCLASSIFIED
CONFIDENTIAL

During this reporting period, the initial formal issue of the spacecraft design book, containing system and subsystem functional requirements, and defining the system design, was completed. The system preliminary design review, including the examination of mission design, the spacecraft and other systems, and the major interfaces, was conducted November 29 and 30. A quarterly project review was conducted December 13, 1966.

Proposals were received for the propulsion subsystem, the television optics and vidicons, and the spacecraft power simulators to be used in scientific instrument testing. Letter contracts were issued to Litton Systems for the data automation subsystem, to Santa Barbara Research Corporation for the infrared radiometer, to Electro-Optical Systems, Inc., for television electronics and integration, and to the University of Colorado for the ultraviolet spectrometer. Definitive Phase I contracts were executed with Honeywell, Inc., for the attitude control subsystem, and with Electro-Optical Systems for the approach guidance subsystem.

B. Project Engineering

1. Launch Vehicle System

a. AC-9 flight. During this report period, results of the *Centaur* R&D flight of *AC-9* became available. *AC-9*, a two-burn mission carrying a *Surveyor* mass model, was successfully launched October 26, 1966. This was the second launch attempt, the first (October 25) having been scrubbed. The flight successfully met the prime objective in demonstrating the capability of coast phase propellant management of the cryogenic system and the subsequent restart of the *Centaur* engines.

Although *Mariner* Mars 1969 will utilize a single burn, direct ascent flight of the *Centaur*, the *AC-9* flight was nevertheless of significant importance to the *Mariner* Mars 1969 program. In addition to confidence gained in the ability to manage cryogenic propellants in space, injection guidance accuracy and *Centaur* retromaneuver capability were again demonstrated.

C. Systems

1. Trajectory Design

The traces of the optic axes on the Martian surface for the various scientific instruments are a function of the aiming point in the **R, T** plane and the pointing angles of the science platform. A set of aiming points about a nominal point is shown in Fig. 1. This view is

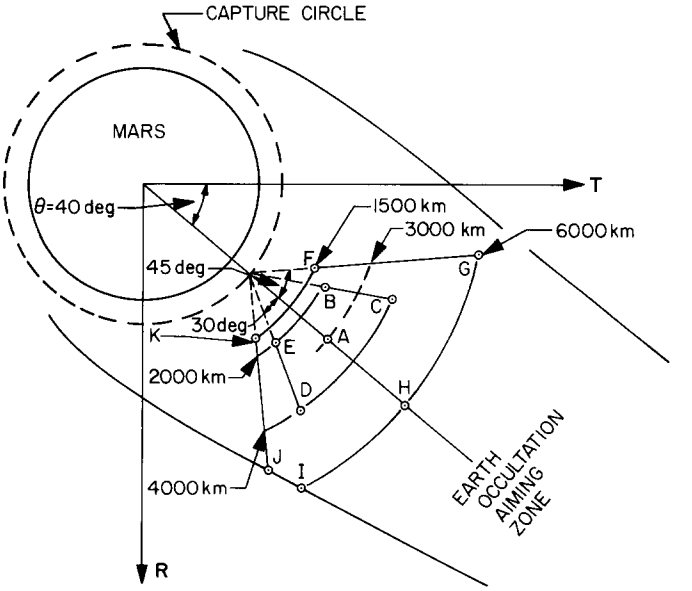

Fig. 1. Aiming point dispersions

along the incoming asymptote, perpendicular to the **R, T** plane, with **T** parallel to the ecliptic. The nominal point A of Fig. 1 is 40 deg down from the **T** axis and corresponds to a closest approach altitude of 3000 km. At this angle from the **T** axis, the TV camera will point in the trajectory plane while viewing 5 deg below the south polar cap (65 deg south latitude). The 3000-km altitude was chosen as nominal in order to achieve the desired picture resolution and amount of frame overlap. The outer fan in Fig. 1 reflects a factor of 2 variation in periapsis altitude, and the 45-deg off-vertical looking angle corresponds to a degradation in TV picture quality of approximately $(1 - \cos 45\,\text{deg}) \approx 30\%$, which is considered to be marginal. The inner fan reflects the experimenters' desire to pass within ± 1000 km from the nominal flyby altitude, and the 30-deg fan corresponds to a degradation of $(1 - \cos 30\,\text{deg}) \approx 14\%$, or about ½ the degradation of the 45-deg off-vertical angle. Points I and J were taken on the boundary of the Earth occultation zone as shown, since a second midcourse maneuver would be performed if the spacecraft trajectory was estimated to lie outside the occultation region.

The scan platform pointing direction is altered as the trace moves across the planet. The initial cone angle is set to achieve approximately 17 min, 30 sec of total TV viewing time, and the clock angle is set to align the ultraviolet (UV) spectrometer parallel to the illuminated limb. Cone angle and clock angle are defined in Fig. 2. At some time after the UV (offset −11 deg in cone angle from the TV) comes on the planet, the platform slews

CONFIDENTIAL
UNCLASSIFIED

UNCLASSIFIED
CONFIDENTIAL

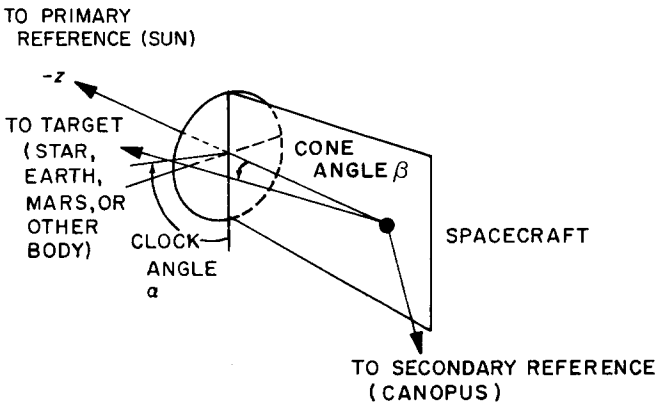

CONE ANGLE (β):
THE ANGLE, MEASURED AT THE SPACECRAFT, BETWEEN THE SUN LINE AND σ LINE THROUGH THE OBJECT OF INTEREST

CLOCK ANGLE (α):
THE DIHEDRAL ANGLE, AT THE SPACECRAFT, FROM THE SUN-SPACECRAFT-CANOPUS PLANE TO THE SUN-SPACECRAFT-OBJECT PLANE MEASURED IN A CLOCKWISE DIRECTION WHEN LOOKING TOWARD THE SUN

Fig. 2. Definition of cone and clock angle

in clock angle to allow the TV trace to travel as far south as 65 deg south latitude.

The platform is then slewed in cone angle to its minimum position (i.e., UV cone angle = 90 deg, TV cone angle = 101 deg). The traces then continue to the terminator and dark-limb crossing. The infrared radiometer is boresighted with the TV and the infrared spectrometer is offset −4 deg in cone angle from the TV. An alternate final platform slew was considered: the minimum cone angle, and the original UVS clock angle are commanded for the final platform slew.

Fig. 3 shows the resulting traces for the nominal case. Points 1–5 define the trace at the initial cone and clock angles as described above. Points 6–9 describe the polar cap pass; points 10–14 show the trace for the final cone slew to 101 deg for the TV. The alternate platform slew is described by points 17–21. The UVS scan trace at the final cone angle of 90 deg is shown by points 15, 16. Points 15A, 16A show the same trace for the alternate platform slew. The angle that the optic axis makes with the local vertical (EMission angle), the supplement of the angle between the Sun vector and the local vertical (INcident angle), and the range along the optic axis to the surface (slant range SR) are tabulated for each point of the trace.

Evaluation by the experimenters of the traces of each dispersed aiming point indicated a preference for an aiming point closer to the vicinity of point B, as opposed to the originally selected nominal aiming point at A. No significant preference was indicated between the final platform clock-angle slew options.

Dispersed aiming points about a nominal point 5 deg below the T axis, at 3000-km periapsis altitude, with different pointing direction schemes, will be the subject of the next dispersed trajectory study.

2. Orbit Determination

Following the analysis presented in SPS 37-39, Vol. III, pp. 18–23, it has been shown that the major factors affecting the capability to achieve the required orbit determination accuracies are station location uncertainties, "effective" doppler noise, and computer program availability.

During the encounter phase of the *Mariner* Mars 1969 mission, currently the most demanding navigational accuracy requirement is that specified by the need for precise pointing of the UV spectrometer. This requirement (translated into navigational accuracy) becomes ±250 km, 3 σ, in a direction perpendicular to the incoming asymptote and to the target-probe line, at least 4 hr before encounter.

The accuracy obtainable is limited by uncertainties in the locations of the tracking stations and by the "effective" quality of the tracking data. This concept of "effective" tracking data quality includes the degradation introduced by the incompleteness of the model used by the computer program to simulate the "real universe."

The extent to which each of these error sources affects the navigational accuracy is dependent upon the computer program to be used. The current Single Precision Orbit Determination Program (SPODP) will be capable of using an "effective" noise, on counted two-way doppler averaged over 1 min, of 3–6 mm/sec. Because of its inadequate model for Earth spin-axis wandering and the imperfect ephemerides, the SPODP will not be able to make use of station location uncertainties below the 5–10-m level, even though it is expected that the station coordinates will be known to within 1.5–3 m by 1969.

The Double Precision Orbit Determination Program (DPODP), now being developed, will be able to utilize data noise levels of 1–3 mm/sec and the actual station location uncertainties of 1.5–3 m.

CONFIDENTIAL
UNCLASSIFIED

UNCLASSIFIED
CONFIDENTIAL

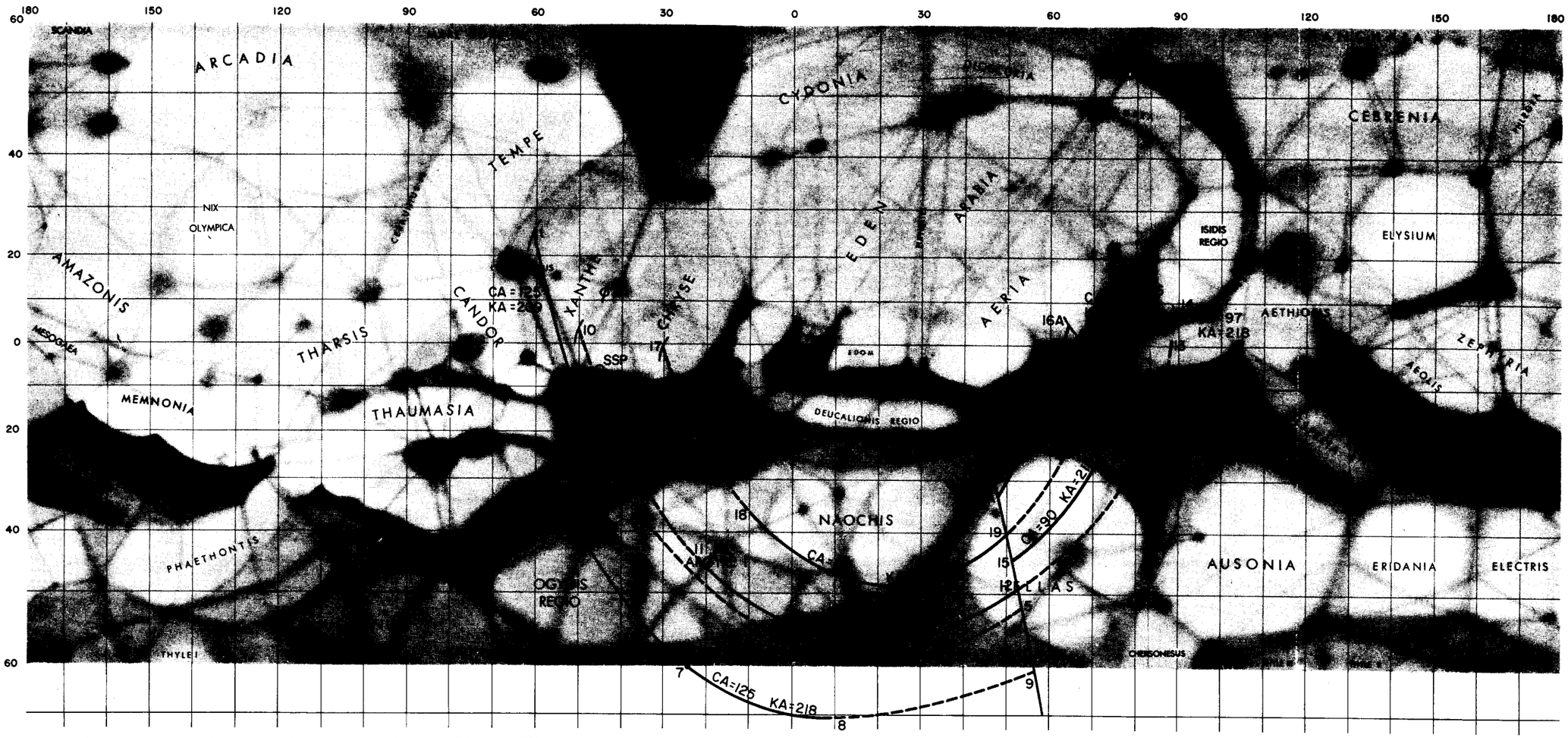

	t	SR	EM	IN		t	SR	EM	IN		t	SR	EM	IN		t	SR	EM	IN		t	SR	EM	IN
1	-17:55	9600	88.7	36.0	5	-3:44	3840	46.0	90.0	10	-9:21	6850	89.4	10.8	15	1:16	3310	30.8	90.0	18	-6:10	4240	46.5	43.5
2	-15:45	6970	49.4	9.1	6	-13:32	5860	36.5	26.5	11	-6:10	4000	37.6	42.0	15A	1:16	3810	52.5	90.0	19	-0:18	3620	46.4	90.0
3	-13:32	5760	32.0	23.5	7	-8:40	4130	1.2	54.5	12	-0:08	3240	28.0	90.0	16	6:11	5880	90.0	129.7	20	2:37	5350	90.0	118.5
3A	-13:32	8200	85.0	20.0	8	-6:10	3690	16.5	70.0	13	4:21	5800	90.0	136.8	16A	4:01	5600	90.0	110.9	21	3:10	5530	90.0	116.5
4	- 7:55	4050	18.1	60.1	9	-3:26	3610	37.8	90.0	14	5:03	5910	90.0	134.8	17	-9:06	6500	84.0	13.0					

Fig. 3. Scan trace for nominal aiming point (θ = 40 deg; B = 7250 km)

CONFIDENTIAL
UNCLASSIFIED

UNCLASSIFIED
CONFIDENTIAL

These levels of uncertainty determine bounds for the accuracies obtainable. Fig. 4 depicts the performance zones to be expected from the two programs.

As can be seen from the figure, the 1-σ uncertainties range from 65 to 130 km for the DPODP, and from 205 to 405 km for the SPODP. Associated with each of these bounds is a probability of achieving the required accuracy. These probabilities are, respectively, 99.6 to 96% for the DPODP and 82 to 48% for the SPODP.

Under the operational conditions expected in 1969, other error sources such as small nongravitational forces, mass-of-Mars uncertainty, and ephemeris errors, should not provide major hindrances in achieving the required accuracy near encounter.

3. Space Guidance Analysis

The analysis and program development effort that has been achieved in the space guidance area for the *Mariner* Mars 1969 project will be summarized here. Numerical results will be presented in a subsequent SPS.

A 1620 computer program has been written with the capability to analyze the effect of midcourse execution errors and Orbit Determination (OD) errors for one- and two-maneuver missions. The covariance matrix of execution errors is determined by an approximation to the Gates model described in Ref. 1. Statistics of the OD errors are included, as are estimates for the random low thrust forces and ephemeris errors. *A priori* uncertainties are combined with execution and OD statistics

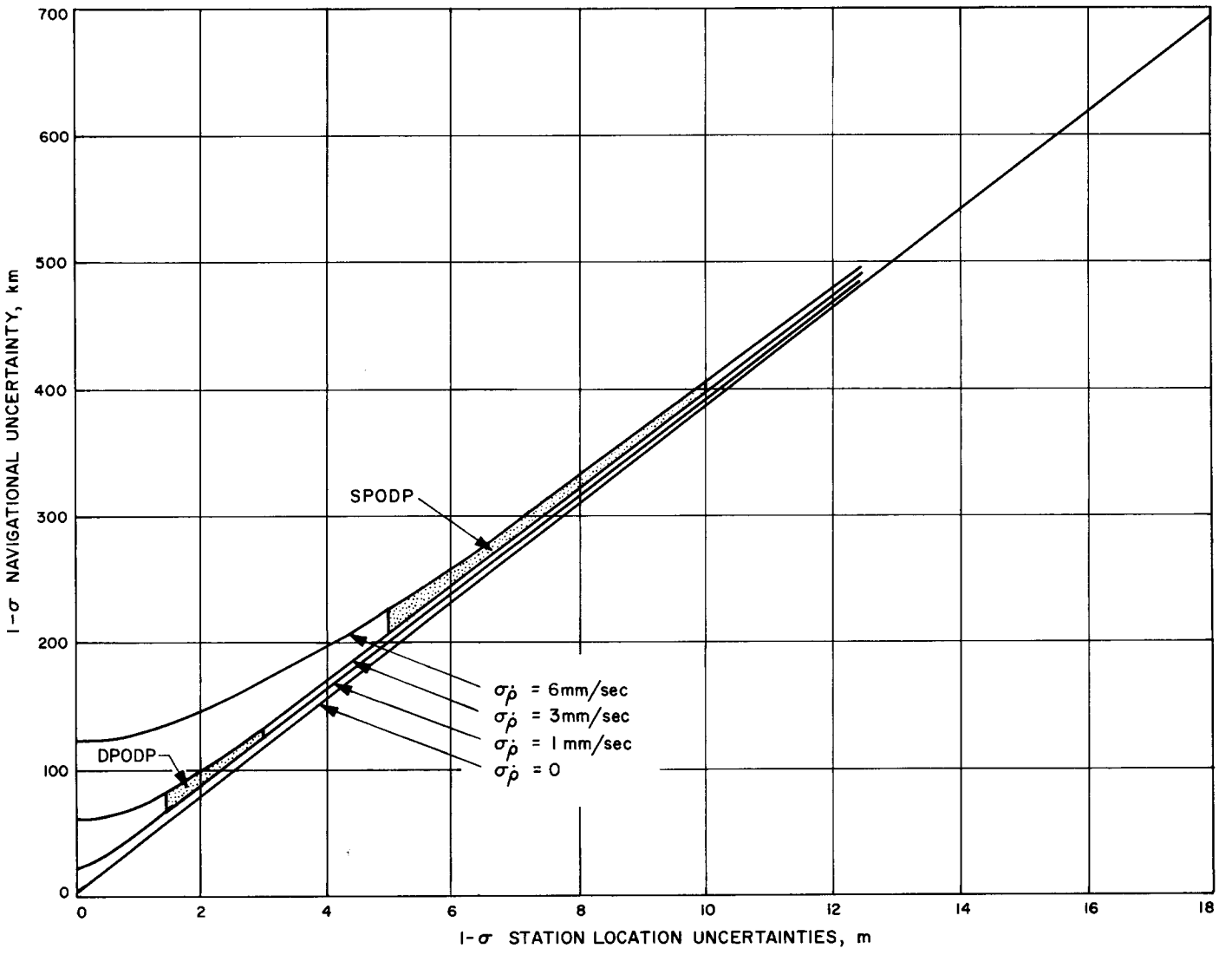

Fig. 4. Navigational accuracy at E — 4 hr as a function of station location uncertainties and effective data noise

UNCLASSIFIED
CONFIDENTIAL

UNCLASSIFIED
CONFIDENTIAL

and epoch forwarded to give the total statistical dispersions at Mars after each maneuver. The aiming point strategy is nonadaptive, i.e., the aiming points are specified at the start of the analysis. However, the aim points for different maneuvers need not be the same.

The total allowable probability of impacting the planet on any given mission is determined by the planetary quarantine constraint. Analysis has been performed to show that, by proper allocation of risk between injection and first maneuver aim points, it is possible to minimize either the final periapsis altitude or the size of the dispersions at the target. A program has been written which determines the radial distance of the injection and first maneuver aiming points for a given angular position and for various levels of quarantine risk allocations. This program is limited in that the angular positions of the two aiming points must be specified as input.

In order to minimize execution errors, it is necessary to minimize the magnitude of the maneuver to be performed. Due to time varying sensitivities of trajectories, various injection aiming points lead to different magnitudes for the total corrective maneuver. A third program has been developed with the capability to determine the angular position of the injection aiming point that leads to a minimum first maneuver velocity.

Current analysis and program development effort is directed toward combining the three programs discussed above into one 7094 program. This program will have all the general analysis capabilities of the first program, and will have the additional capability to determine optimum aiming points in the sense of minimum errors for a specified final aiming point.

4. Mission Analysis

a. Mission Plan and Requirements Document. The Mission Plan and Requirements Document, PD-91, describes the *Mariner* Mars 1969 mission and states the technical requirements placed upon the project systems to fulfill project objectives. A draft of the document was presented to the system preliminary design review conducted in December. System and general reviews are under way, and release of the document is expected in the next report period.

b. Mission success studies. The purpose of mission success studies is to evaluate mission mode and system implementation options to assist the *Mariner* Mars 1969 Project Office in selecting those options which result in the highest level of mission success. Studies will be made to determine which are the critical areas and how they can be strengthened or, possibly, if areas exist that are receiving too much emphasis, how they should be deemphasized.

The mission success studies will account for the design of the systems and will include the reliabilities of key mission events. These studies will be computerized wherever possible.

5. Planetary Quarantine

NASA has specified that certain precautions be taken to ensure a high probability that Mars will not be contaminated with terrestrial organisms prior to the successful completion of an adequate spectrum of biological experiments. The need to perform a large number of experiments will require that many missions be flown to Mars; thus the probability of Mars contamination by any single mission must be held to a very small number.

It is, of course, essential to define what is meant by the term "contaminated." It is possible to impact Mars with either large populations of organisms (unsterilized *Centaur* stage or *Mariner* spacecraft) or very small populations (various effluxes such as attitude control gas, spalling, outgassing, propulsion system exhaust, and micrometeoroid ejecta). In regard to the former category, impact shall be assumed tantamount to contamination, even though it is felt by many investigators that the Martian environment is sufficiently hostile to terrestrial organisms (even in large populations) so as to result in a low probability of survival and replication. In regard to the second category, concerning single or very small organism populations, impact shall not be interpreted as tantamount to contamination. In fact, the probability of contamination by small particles containing only a few organisms shall depend upon the product of a number of probabilities such as:

(1) being released from the spacecraft or launch vehicle

(2) being viable at the time of release

(3) surviving the ejection process

(4) achieving an impact course in the presence of solar radiation pressure

(5) surviving the ultraviolet radiation during cruise to the planet

(6) surviving atmospheric entry heating

UNCLASSIFIED
CONFIDENTIAL

UNCLASSIFIED
CONFIDENTIAL

(7) being released into the Martian environment

(8) surviving and multiplying in the Martian environment

The total allowed probability of Mars contamination by the 1969 mission must be allocated between the two launches and, for each launch, among the *Centaur*, the spacecraft, and the efflux sources.

An analysis of the planetary quarantine requirement and its effect on the *Mariner* Mars 1969 mission has recently been performed at the request of NASA Headquarters. Highlights of this analysis are presented here.

a. Mission considerations of large population sources of contamination. To satisfy the mission requirements, it is necessary that the spacecraft pass through a particular region of space near Mars. The geometry is illustrated in Fig. 5. The plane of Fig. 5 represents the plane which is perpendicular to the hyperbolic approach asymptote as the spacecraft nears the planet; the R and T axes are mutually perpendicular and also perpendicular to the approach asymptote, with T parallel to the plane of the ecliptic.

Meetings with the principal investigators have led to selection of two primary areas of interest on Mars for the 1969 mission:

(1) the regions near (above and below) the edge of the south polar ice cap

(2) the light and dark regions between 10 deg north and 30 deg south latitude

To achieve a flyby trajectory which results in occultation by Mars of the radio signal and also allows adequate viewing of the regions near the ice cap, the spacecraft approach asymptote must pierce the R-T plane of Fig. 5 near 40 deg (measured clockwise from the T axis). The alternate area, from 10 deg north to 30 deg south, requires an aim point of approximately 5 deg. There is general agreement among the principal investigators that the results of the scientific experiments will have the most value if the closest approach altitude is 3000 km. A deviation of more than approximately 1000 km in either direction results in some loss in value. The two wedge-shaped areas shown in Fig. 5 straddle the 40-deg line, with the smaller wedge centered at a point corresponding to a closest approach altitude of 3000 km. Thus they represent target zones in the R-T plane associated with the former of the two regions of interest on Mars.

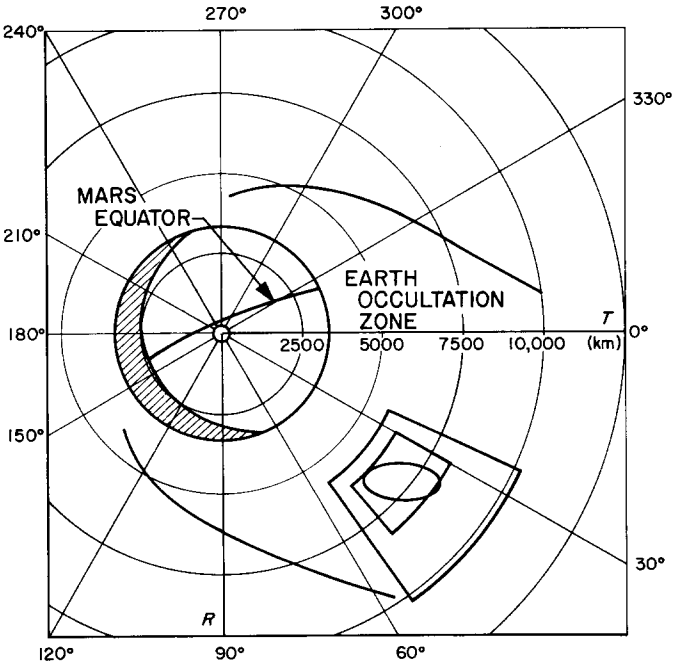

Fig. 5. Aiming geometry

Characteristics of the two zones are:

	$\theta_{minimum}$, deg	$\theta_{maximum}$, deg	$h_{p_{minimum}}$, km	$h_{p_{maximum}}$, km
Small zone	30	50	2000	4000
Large zone	25	55	1500	6000

θ is the polar angle in the R-T plane, and h_p is the flyby trajectory periapsis altitude.

Guidance philosophy. Since the launch vehicle and the spacecraft are not guided perfectly, dispersions from the nominal aiming point in the R-T plane will exist. If these dispersions are of sufficient size to cause the probability of impact requirement to be violated, the aiming point must be biased away from the planet a distance sufficient to satisfy the requirement.

In the case of injection aiming, it will be necessary to bias the aiming point. This is illustrated in Fig. 6, which is a contour in the R-T plane associated with a particular probability that the combination of launch vehicle aiming and the unreliability of subsequent events (namely, launch vehicle retro and spacecraft first maneuver) will result in impact. The unreliabilities shown on Fig. 6, i.e., q_R (retro) = 0.03 and q_1 (first maneuver) = 0.03, are based on current best estimates of launch vehicle and spacecraft event reliabilities. The launch vehicle can be aimed

CONFIDENTIAL
UNCLASSIFIED

UNCLASSIFIED
CONFIDENTIAL

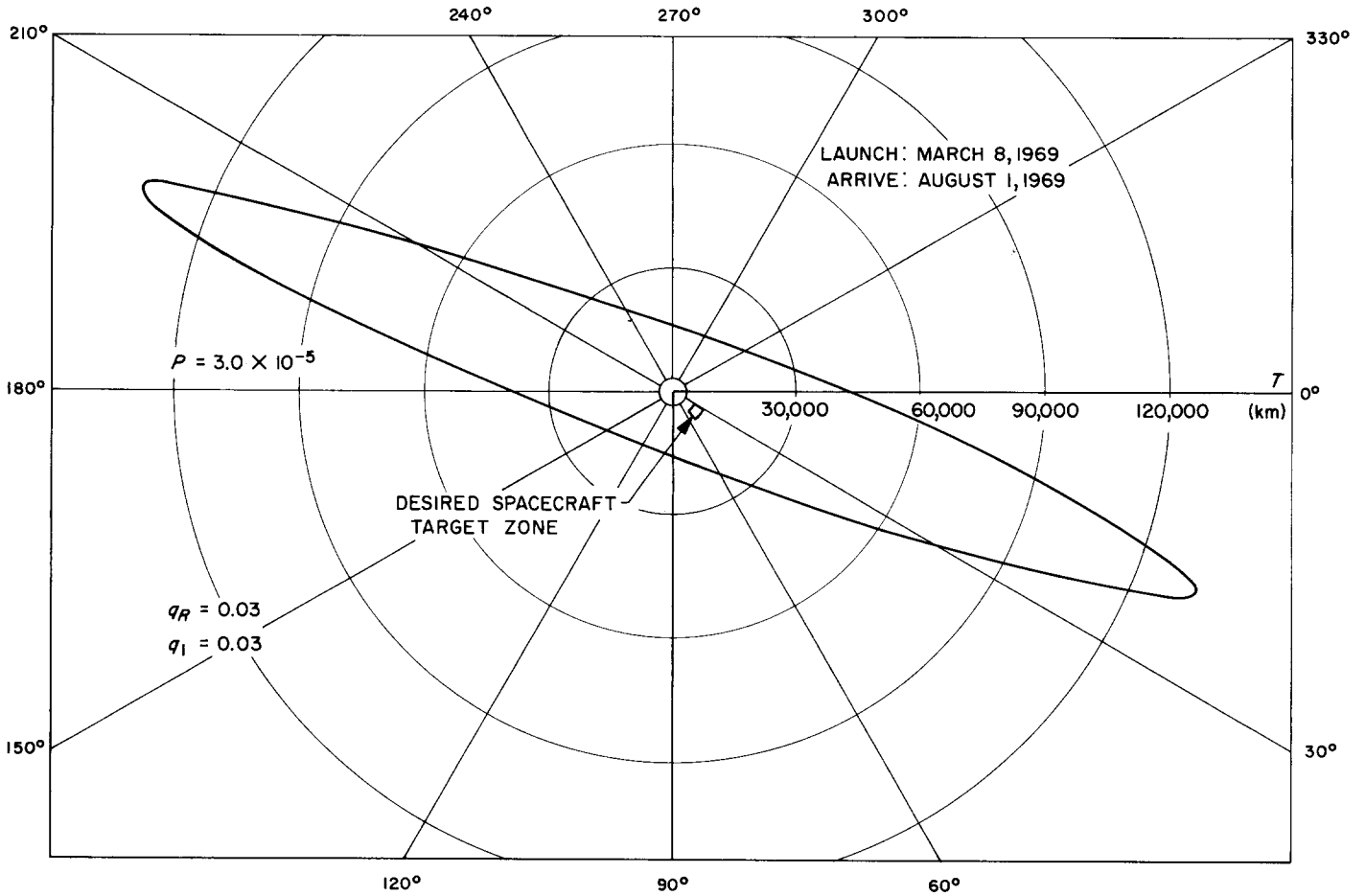

Fig. 6. Probability of impact contour at injection

anywhere on or outside the locus to satisfy the particular requirement indicated (i.e., $P = 3 \times 10^{-5}$).

As the injection aim point is biased further from the desired aim point, the magnitude of the spacecraft trajectory correction maneuver is increased. Several sources of spacecraft guidance inaccuracy are proportional to the size of the maneuver; the result of this guidance inaccuracy is an increase in the *a priori* dispersions about the spacecraft maneuver aim point in the *R-T* plane. Once the location, size, and orientation of the spacecraft maneuver ellipse are known, the probability that the spacecraft approach asymptote will pass through a desired region in the *R-T* plane can be determined. As the expected size of the spacecraft maneuver dispersion ellipse increases, the probability that the spacecraft approach asymptote will pass through the desired region decreases. The same effect holds if the spacecraft maneuver aiming point must be biased away from the desired aiming point. If, after the spacecraft trajectory correction maneuver is performed, it is determined by tracking that the spacecraft will not pass through the desired region in the *R-T* plane, a second maneuver will be required.

Results. The probability of requiring a second maneuver is equivalent to the probability that the spacecraft approach asymptote will not pass through the desired region. This probability is illustrated in Fig. 7 as a function of launch date for an assumed August 1 arrival, assuming three different quarantine levels and the current estimates of launch vehicle retro and spacecraft first and second maneuver reliabilities. The dashed lines, labelled "no constraint," represent the probability of requiring a second maneuver to reach the target zone if the quarantine requirement were removed; they indicate the effect of the inherent (unbiased) guidance inaccuracies. The small and large zones of Fig. 7 refer to the two regions of Fig. 5.

Fig. 7 shows that the probability of requiring a second maneuver is much higher early in the launch period and decreases steadily throughout the period for all three

UNCLASSIFIED
CONFIDENTIAL

UNCLASSIFIED
CONFIDENTIAL

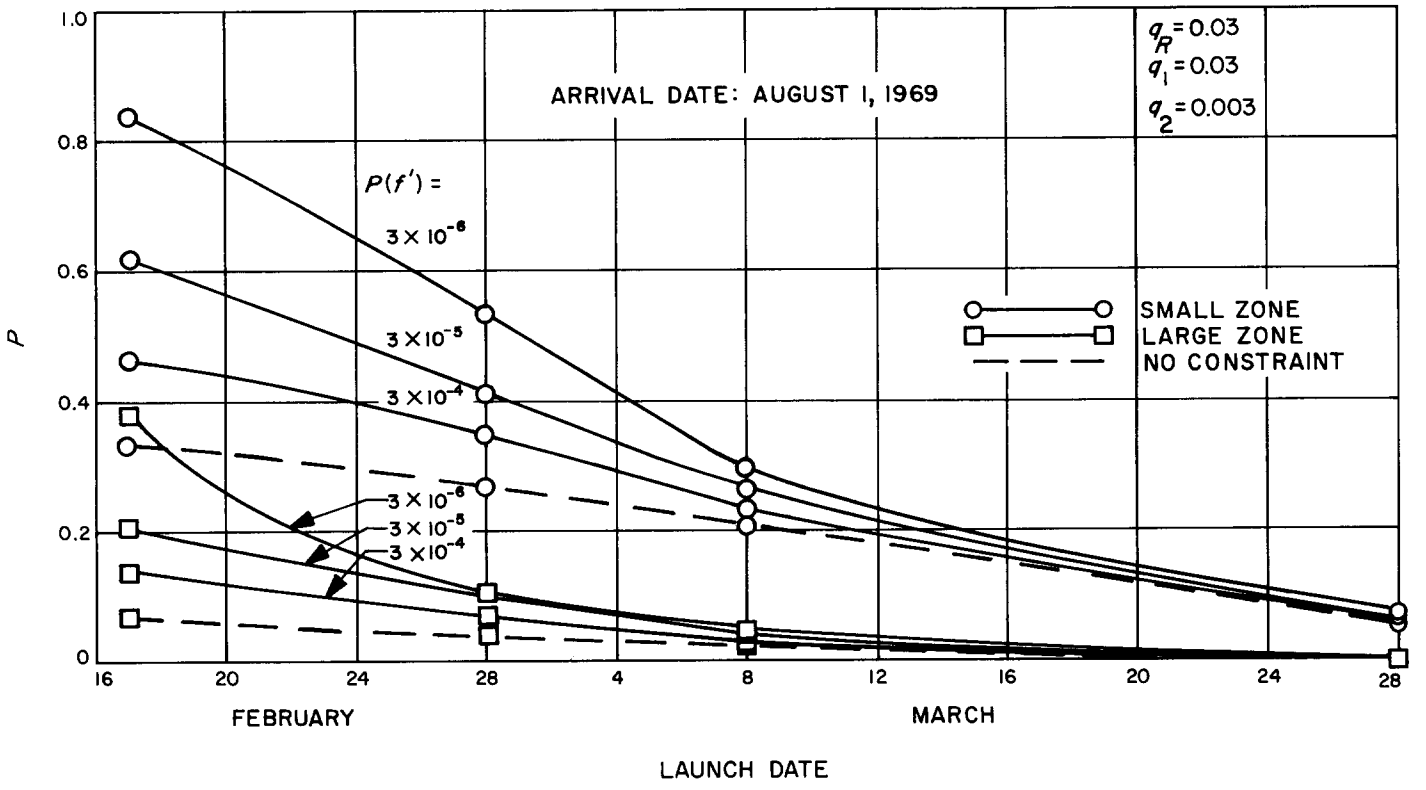

Fig. 7. Probability of requiring a second maneuver to hit target zone as a function of launch date

levels of quarantine. In addition, this probability has a marked sensitivity to the quarantine level early in the launch period but, by approximately mid-March, this sensitivity has decreased significantly. Thus, a rational policy would allocate a significantly larger portion of the total mission quarantine allowance to the first launch than to the second launch, so as to reduce the probability of requiring a second trajectory correction for the first launch without appreciably affecting the second launch. Typical allocations might be 5.0×10^{-5} and 1.0×10^{-5} probability of impact for the first and second launches, respectively.

Method of analysis. Fig. 7 is based upon an optimization procedure. For a particular launch and arrival date combination, the probability of contamination with large population sources can be approximated by:

$$P(f') \approx P(f_i') [q_R + q_1] + P(f_1') q_2 \qquad (1)$$

where

$P(f')$ is the probability of contaminating Mars due to launch vehicle or spacecraft impact

$P(f_i')$ is the probability that the launch vehicle injects the *Centaur* and spacecraft on an impact trajectory

$P(f_1')$ is the probability that the spacecraft first maneuver results in an impact trajectory

q_R, q_1, and q_2 are the probabilities that *Centaur* retro and the spacecraft first and second maneuvers fail

The assumptions upon which the simplified Eq. (1) is based are:

(1) the probability of launch vehicle impact, given that *Centaur* retro has occurred, is negligible

(2) the probability that a spacecraft maneuver is required is essentially unity

(3) the probability of spacecraft impact, given that two maneuvers have occurred, is negligible

(4) the probability that the second maneuver is available, given that the first was not available, is essentially zero

(5) the separation velocity between the *Centaur* and the spacecraft is close to zero

UNCLASSIFIED
CONFIDENTIAL

UNCLASSIFIED
CONFIDENTIAL

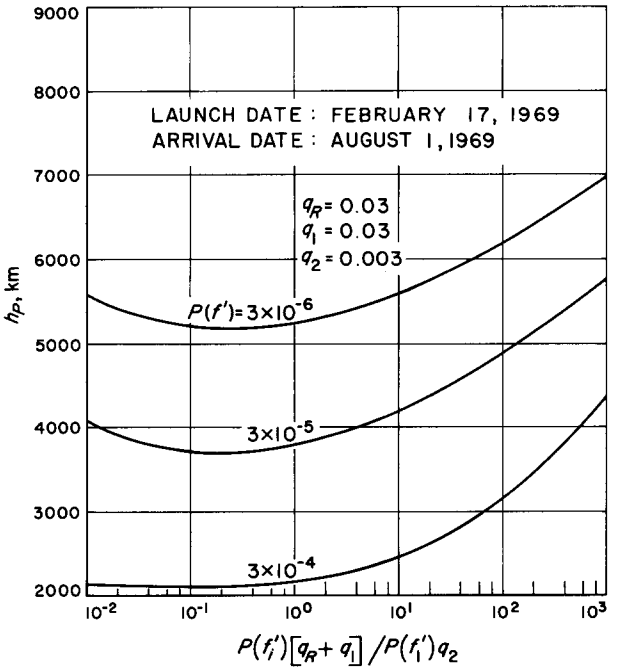

Fig. 8. Closest approach aim point versus apportionment of risk

For a given set or $P(f_i')$, $P(f_1')$, q_R, q_1, and q_2, the spacecraft first maneuver aim point and expected dispersions about the aim point are determined, based upon Eq. (1), as discussed previously. If $P(f')$, q_R, q_1, q_2 are held constant and $P(f_i')$ and $P(f_1')$ allowed to vary, the spacecraft first maneuver aim point and the associated dispersion ellipse will vary. Examples of this variation are given in Figs. 8 and 9, which are used together to select the optimum combination of spacecraft first maneuver aim point and the associated *a priori* dispersion ellipse. Fig. 8 shows the allowable periapsis altitude corresponding to the aim point of the approach asymptote as the apportionment between $P(f_i')$ and $P(f_1')$ varies for three values of $P(f')$. Fig. 9 illustrates the variations in the expected values of the semimajor and semiminor axes of the dispersion ellipse for the same three values of $P(f')$. Both figures are for a launch date of February 17 and an arrival date of August 1. Note that the first maneuver dispersion ellipse (Fig. 9) decreases steadily as more of the risk is apportioned to injection (increasing $P(f_i')/P(f_1')$). However, the allowable periapsis altitude (Fig. 8) dips and then rises. If the value of allowable h_p dips below 3000 km (the altitude which has the highest value according to the principal investigators) we select that value of $P(f_i')/P(f_1')$ which gives $h_p = 3000$ km with positive slope, since this corresponds with the desired aim point and the smallest dispersion ellipse. A higher value of $P(f_i')/P(f_1')$ causes the spacecraft maneuver aim point to be biased, while a smaller value results in a larger dispersion ellipse. If the value of allowable h_p does not reach 3000 km, the value of $P(f_i')/P(f_1')$ corresponding to the minimum allowable h_p is selected.

Having selected the aim point and the corresponding dispersion ellipse, it is then necessary to determine the probability that the spacecraft will pass through the target zone. Assuming that the dispersions about the aim point will have Gaussian distribution along both the semimajor and semiminor axes, this probability can be expressed as:

$$P(T) = \frac{1}{2\pi\sigma_a\sigma_b}\int_{a_1}^{a_2}\int_{b_1}^{b_2}\exp\left\{-\frac{1}{2}\left[\left(\frac{a}{\sigma_a}\right)^2+\left(\frac{b}{\sigma_b}\right)^2\right]\right\}db\,da \tag{2}$$

where

$P(T)$ is the probability of hitting the target zone

σ_a and σ_b are the standard deviations of the semimajor and semiminor axes, respectively

a_1, a_2, b_1, and b_2 are the limits of the target zone with respect to the orientation of the maneuver dispersion ellipse

CONFIDENTIAL
UNCLASSIFIED

UNCLASSIFIED
CONFIDENTIAL

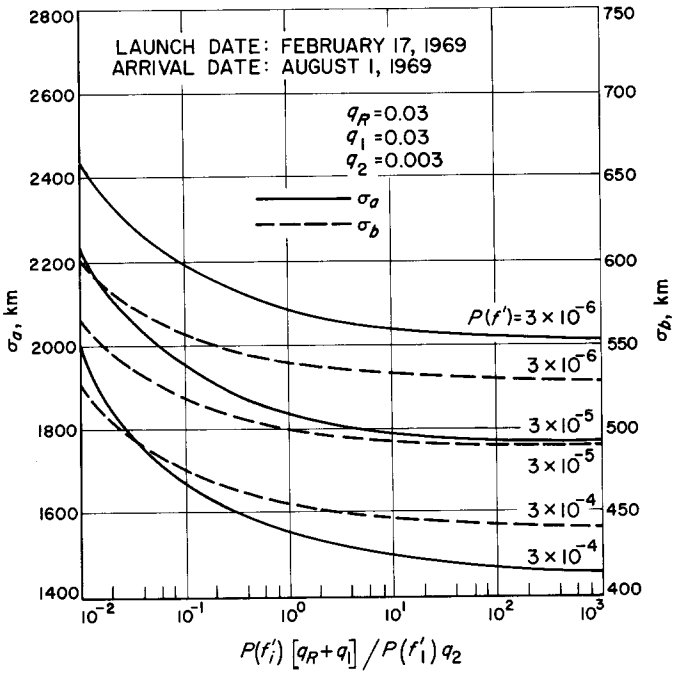

Fig. 9. Variations in the expected values of the semimajor and semiminor axes of the spacecraft first maneuver dispersion ellipse

b. Small population sources of contamination. There are basically five ways of contaminating Mars with launch vehicle and spacecraft ejecta products. They are: *Centaur* blowdown ejecta; outgassing; attitude control ejecta; midcourse motor exhaust products; micrometeoroid ejecta.

The first two are considered to be negligible sources of contamination, as are midcourse motor exhaust products.

Analysis conducted for the *Mariner* Mars 1964 mission indicated that the probability of any organisms from the attitude control subsystem contaminating Mars was less than 10^{-8}. Since the *Mariner* Mars 1969 spacecraft uses the same attitude control subsystem including the same filters, it is assumed that the probability of attitude control gas contaminating Mars will not exceed 10^{-8}.

In estimating the probability of contaminating Mars by material ejected from the spacecraft by micrometeoroid impacts, use was made of studies conducted in this area for the *Voyager* Project by the Boeing Company. This probability of contamination is computed to be approximately 6×10^{-8}.

It is considered unlikely that spacecraft or launch vehicle ejecta will result in a probability of contamination greater than 10^{-6}.

c. Recommendations for the Mariner Mars 1969 quarantine requirements. In light of the results, the following recommendations were made to NASA Headquarters:

Large population sources of contamination. Since the probable necessity of having to perform a second trajectory correction is much more sensitive to the quarantine level early in the launch period than it is later, it was recommended that the planetary quarantine requirement be stated to apply to the launch opportunity as opposed to each launch. This would allow more flexibility in mission design. An example might be to apportion a total probability of contamination of 6×10^{-5} to the opportunity, with the probability of contamination set at 5.0×10^{-5} for the first launch. This would allow the first spacecraft to be launched as early as possible with the lowest realizable probability of needing a second maneuver. The remaining 1.0×10^{-5} would be apportioned to the second launch, etc.

Small population sources of contamination. It is recommended that the value of $P(r')\,P(g')$ be assumed to be less than 1.0, with the value for each source of contamination to be determined through analysis and research, where $P(r')$ and $P(g')$ are the probabilities that a population of viable organisms will be *released* and will *grow*, respectively, given that impact has occurred. It is desired that the various studies pertaining to the *Voyager* Project be directed in such a manner that some of their results are applicable to the *Mariner* Mars 1969 Project.

Over-all requirement. It is requested that the early assumption (70 landers and 30 flybys over the 20-yr period beginning in 1964), upon which the present quarantine allowance of 3.0×10^{-5} per launch is based, be reexamined. Current OSSA planning suggests that there may be fewer spacecraft flown to Mars during this period.

d. Quarantine criteria established by NASA Headquarters. As a result of the analysis and other studies, the following set of criteria has been established for the *Mariner* Mars 1969 mission:

(1) The probability of contaminating Mars shall not exceed 6.0×10^{-5}, with the maximum probability for an individual flight being 5.9×10^{-5}.

(2) The value of $P(r')$ shall be assumed to be unity.

(3) The value of $P(g')$ shall be assumed to be unity.

CONFIDENTIAL
UNCLASSIFIED

UNCLASSIFIED
CONFIDENTIAL

D. Guidance and Control

1. Central Computer and Sequencer Subsystem

Testing of the *Mariner* Mars 1969 CC&S breadboard has accelerated rapidly since the last report in SPS 37-42, Vol. II. About 400 hr of test time have been accumulated to date with nearly one-half of this time spent at temperature extremes of −10 to +85°C with voltage extremes of ±20%. Design performance has been weak in only two areas: performance margins of the magnetic memory and injected noise sensitivity of monostable multivibrators. The memory has been subjected to rigorous worst-case design analysis and the performance problems are now understood. A new design correcting these deficiencies has been generated and a new breadboard memory is 80% complete. The sensitive monostable multivibrators have been replaced by gated counter techniques in the computer timing logic and have been masked by less sensitive circuitry in the peripheral input–output logic.

A contract to document and fabricate a flight prototype CC&S was initiated December 12, 1966 with Motorola's Military Electronics Division/Western Center. This contract requires detail packaging design and fabrication documentation, the fabrication of one flight prototype, and testing below the subsystem level. Subsystem temperature-voltage margin tests and environmental tests will be conducted at JPL with Motorola assistance. The prototype is to be delivered in May 1967 with test completion anticipated by mid-July 1967.

2. Spacecraft Control

Definitive research and development contracts have been signed with Honeywell, Inc., for *Mariner* Mars 1969 attitude control and scan control and with Electro-Optical Systems for approach guidance.

Functional requirement documents for the attitude control, scan control, and approach guidance subsystems have been released.

All approach guidance interface circuits have been defined and the circuit data sheet material has been completed.

Preliminary parts lists for the attitude control and approach guidance subsystems have been submitted to Project Reliability Assurance.

Attitude control interface circuit definition is 75% complete. Design room activity has started for modifications to the attitude control electronic design. These modifications are generally to accommodate the new Canopus sensor logic.

Breadboard activity has started for the scan control electronics, the far-encounter planet sensor, and the Canopus sensor.

Reference

1. Gates, C. R., *A Simplified Model of Midcourse Maneuver Execution Errors,* Technical Report 32-504, Jet Propulsion Laboratory, Pasadena, California, October 15, 1963.

CONFIDENTIAL
UNCLASSIFIED

UNCLASSIFIED
CONFIDENTIAL

III. *Voyager* Project

A. Introduction

1. Objectives

The primary objective of the *Voyager* Program is to carry out scientific investigations of the solar system by instrumented, unmanned spacecraft which will fly by, orbit, and/or land on the planets. Emphasis will be placed on acquisition of scientific information relevant to the origin and evolution of the solar system; the origin, evolution, and nature of life; and the application of this information to an understanding of terrestrial life. The primary objective of the *Voyager* missions to Mars, beginning in 1973, is to obtain information relative to the existence and nature of extraterrestrial life; the atmospheric, surface, and body characteristics of Mars and the planetary environment by performing automated experiments on the surface of, and in orbit about, the planet. A secondary objective is to further our knowledge of the interplanetary medium between the planets Earth and Mars by obtaining scientific and engineering measurements while the spacecraft is in transit.

2. Project Plan

All *Voyager* missions will be conducted as events of an integrated program in which each individual flight forms a part of a logical sequence in an over-all technical plan of both lander and orbital operations. The *Voyager* design will provide for the carrying of large scientific payloads to the planet, the telemetering of a high volume of data back to Earth, and long useful lifetimes in orbit about the planet and/or on the planetary surface. Hardware will be designed to accommodate a variety of spacecraft and/or capsule science payloads, mission profiles, and trajectories. Particular emphasis will be given to simple and conservative designs, redundancy wherever appropriate, and a comprehensive program of component, subsystem, and system testing.

Over-all direction and evaluation of the *Voyager* Program is the responsibility of the Office of Space Science and Applications (OSSA) of the National Aeronautics and Space Administration (NASA). Management of the *Voyager* Project and implementation of selected systems is the responsibility of the Jet Propulsion Laboratory (JPL) of the California Institute of Technology.

3. Technical Description

Planning shall be based upon launching two identical planetary vehicles by a single *Saturn V* launch vehicle

UNCLASSIFIED
CONFIDENTIAL

UNCLASSIFIED
CONFIDENTIAL

at each Martian opportunity, starting with the 1973 opportunity. Each planetary vehicle is to consist of a flight spacecraft, flight capsule bus, and surface laboratory, with science experiments conducted in 1973 from the orbiter, during descent and on the planetary surface. The flight spacecraft with its capability for a 400-lb science subsystem (250 lb of instruments) will weigh aproximately 2,500 lb; its retropropulsion subsystem may additionally weigh up to 15,000 lb; and the total flight capsule (capsule bus and surface laboratory) will weigh up to 5,000 lb. The flight spacecraft will be a fully attitude-stabilized device utilizing celestial references for the cruise phase, and will be capable of providing velocity increments for midcourse trajectory corrections and for Mars orbit attainment by both the flight spacecraft and the flight capsule. On-board sequencing and logic and ground command capability will be provided. The flight spacecraft will supply its own power from solar energy or from internal sources and will be capable of maintaining radio communications with Earth. In addition, the flight spacecraft will be thermally integrated and stabilized and will monitor various phenomena near Mars and during transit, and will telemeter this information back to Earth; it will monitor and telemeter data pertaining to spacecraft operations. The flight spacecraft will also provide the flight capsule with services such as power, timing and sequencing, telemetry, and command during the transit portion of the missions and may serve as a communications relay. The sterilized flight capsule bus will be designed for separation from the flight spacecraft in orbit, for attaining a Mars impact trajectory, for entry into the Martian atmosphere, for descent to the surface, and for soft-landing the surface laboratory, which will have surface lifetimes of up to 2 days in 1973 and later goals of as much as 6 mos. The flight capsule bus will contain the propulsion, guidance, control, communications, and data handling systems necessary to complete its mission, while the surface laboratory will contain all power, sequencing, and communications for the conduct of surface operations.

No deep-space flight tests of the flight spacecraft are planned, and compensation will be made by more extensive ground tests to the extent possible. The test program for the flight capsule, which is planned to include Earth-entry flight tests, will investigate entry dynamics.

During the capsule Phase B time period, assessment shall be made of the quantitative effect of various growth factors on useful landed weight including increases in launch vehicle performance, increase in minimum Martian surface pressure, and availability of current weight contingency.

4. Sequence of Events

The Project plan is being implemented as follows:

The Spacecraft System procurement activity (Task C) is continuing with the three Phase B fixed-price contracts for the accomplishment of mission, system, and management studies. One system contractor will be selected, through competition, for award of a CPAF Phase C contract and, subsequently, a multiple-incentive CPIF-type Phase D contract.

The procurement action for the total capsule system includes selection of multiple Phase B contractors in the last quarter of FY 67 and subsequently, from among these, one Phase C and D contractor for the capsule bus system will be selected to carry out, essentially in parallel, Phases C and D of the spacecraft system procurement. The surface laboratory Phase C procurement will be open competition for one contractor who will carry out Phases C and D.

B. Guidance and Control

1. Proposed Guidance Scheme for a Martian Soft-Landing Vehicle

a. Introduction. The design of the terminal descent system for a Martian propulsive lander presents a challenging technological problem to the engineering community. Unlike the lunar landing vehicle, *Surveyor*, a Martian lander must override the complications induced by the relatively unknown atmosphere on Mars. The atmospheric uncertainty poses the most significant challenge and thus necessitates a design that possesses the capability of successful operation over a considerable range of atmospheric conditions.

On this premise, a recent study was made to define and analyze some of the terminal guidance system problem areas anticipated on a Martian lander mission. An earlier study had been conducted along similar guidelines and the formulation of a terminal descent guidance law resulted. One asset of this law is its ability to bring the vehicle to a zero velocity and a vertical orientation at the surface by modulating the thrust during the descent. However, it remained to be proved that the guidance law possessed the flexibility required.

Initially, the concern was to establish realistic parametric ranges for a lander mission. This included defining the atmospheric entry conditions and the expected atmospheric variations. These determinations provide sufficient information to define the ballistic descent trajectory which,

UNCLASSIFIED
CONFIDENTIAL

UNCLASSIFIED CONFIDENTIAL

in turn, provides the ignition conditions for the propulsion system. Once the ignition conditions are known, the operating range of the terminal descent system is essentially specified.

During the course of the study, it was discovered that a potential fuel consumption problem existed if the descent was in a dense atmosphere. The problem was attributable to the ignition criterion and to the mechanization of the guidance law. Because of the relative simplicity of the ignition criterion, an alternate mechanization of the guidance law was sought. It is the concern of this article to identify further the problem and present a mechanization which affords a feasible solution to the problem.

2. Atmospheric Entry Conditions

Atmospheric entry of the lander is assumed to occur at an altitude of 800,000 ft above the Martian surface. The particular deorbit vacuum trajectory conditions at 800,000 ft provide the initial conditions for the atmospheric descent. Basically, these are the entry velocity, the entry angle (positive in the clockwise direction from the local horizontal), and the entry angle of attack.

The particular entry "corridor" established for this study was:

Entry velocity	13,000 to 15,000 ft/sec
Entry angle	-14 to -20 deg
Entry angle of attack	± 5 deg

The range of entry velocity results from the orbital variations considered. Entry angle bounds are determined by the "skip limit"; that is, the entry angle below which the capsule attains positive flight path angles, and the ballistic velocity magnitude which is, in the region of retro ignition, a function of the entry angle magnitude. The entry angle of attack range is a measure of the lander's capability to align its roll axis with the velocity vector at entry.

It is desirable from the landing point of view to impose rigid constraints on the entry conditions, especially the entry angle and the entry angle of attack. Large deviations from a zero angle of attack at entry may result in prominent aerodynamic oscillations during the descent; the effects of small variations in entry angle on the descent trajectory will be illustrated in the following section. Both of these occurrences require much attention in the design of the terminal descent system.

3. Low Altitude Ballistic Trajectories

The low altitude ballistic trajectory defines the capsule position and velocity in the retro ignition altitude region. Confinement to this region is sufficient to determine the essential requirements of the terminal guidance and control system, the on-board radar system, and the propulsion system.

Trajectory data are dependent on the capsule configuration, expected atmospheric variations, and entry conditions. In particular, the configuration selected was a 60-deg blunted cone forebody and a frustum of a 30-deg cone for the aftbody. The capsule had a ballistic coefficient of 0.3 slugs/ft^2. Assumed atmospheric variations were as defined by Martian models VM-1 to -10, encompassing a surface pressure variation of 5 to 20 mb.

Fortunately, the lander system operational limits can be established by considering only the bounding atmospheric models, maximum entry velocity condition, and entry angle extremities. Low altitude behavior is relatively insensitive to entry velocity variations and VM-7, -8, and -10 form the atmospheric model bounds for our purposes. VM-7 is the most tenuous atmosphere, resulting in the highest capsule terminal velocity; the capsule flight path angle, referenced to the horizontal, is the smallest in VM-8; and VM-10 is the most dense atmosphere.

Shown in Fig. 1 are the limiting trajectories for the conditions cited above. Altitude is plotted as a function of velocity with flight path angle shown adjacent to the circled data points. Important notes about the data are that it is wind-free and computed from a 3 degrees-of-freedom, point-mass computer simulation. Wind effects, such as a continuous wind speed, wind gusts and shear, can alter considerably the trajectories in Fig. 1; however, consideration will not be given to these effects at this time.

The data of Fig. 1 is the basis for determining the retro ignition conditions once an ignition criterion is established.

4. Retro Ignition Conditions

Retro ignition conditions will be defined as the altitude, velocity, and path angle at which the engines are ignited. Ideally, we would like ignition to occur at some altitude sufficient to ensure nominal flight characteristics and minimum impact conditions. Igniting at an excessive altitude may present fuel consumption problems and, conversely, igniting too close to the surface may result in

UNCLASSIFIED CONFIDENTIAL

UNCLASSIFIED

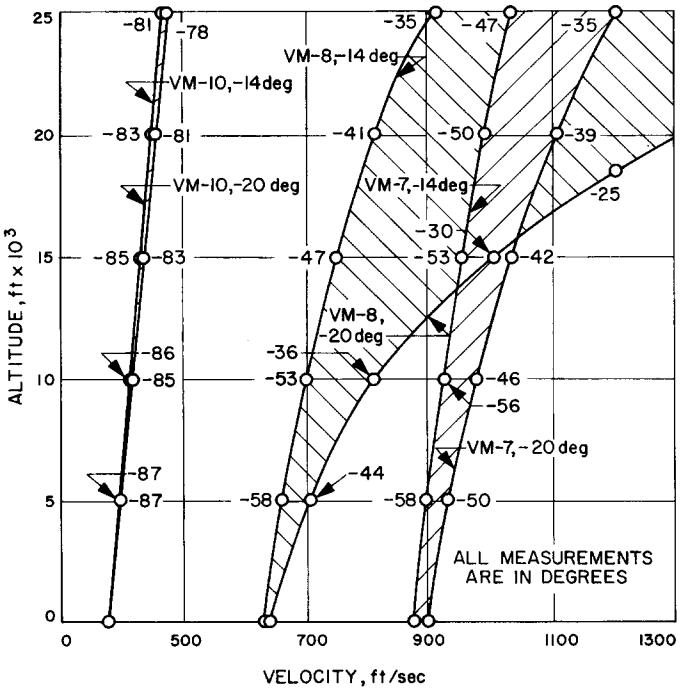

Fig. 1. Low altitude ballistic trajectory envelopes for entry angles of −14 and −20 deg

thrust requirements that exceed the propulsion system capabilities. To circumvent such occurrences, ignition altitude must be controlled to within some predetermined range.

In this study, the criterion established for ignition was to ignite the engines when the slant range equalled a preprogrammed slant range value in the system. When this value is reached, a marking pulse is generated which ignites the engines and initiates the terminal descent. A slant range of 20,000 ft was selected and the ignition conditions (Table 1) were computed at this slant range.

Table 1. Ignition conditions at 20,000 ft slant range

Entry angle: −14 deg		Entry velocity: 15,000 ft/sec	
Atmosphere	Altitude, ft	Velocity, ft/sec	Path angle, deg
VM-7	15,800	960	−52
VM-8	14,600	730	−47
VM-10	19,900	440	−83
Entry angle: −20 deg		Entry velocity: 15,000 ft/sec	
VM-7	13,900	1020	−44
VM-8	11,500	850	−35
VM-10	19,800	445	−81

As shown in the table, significant variations exist in ignition conditions over the atmospheric model range. One interesting aspect resulting from the ignition criterion is that ignition altitude increases as the atmospheric density increases, an event contrary to the desirable.

5. Terminal Guidance System Development

The primary function of the terminal descent guidance system on board the lander is to aid in the assurance that a successful landing will be achieved. The fact that a wide range of ignition conditions exists complicates considerably the guidance system design and, in turn, implies that the thrust capability must be effectively and efficiently utilized to soft-land the vehicle. The proposed guidance system, used in conjunction with an on-board attitude control system, has the flexibility and capability to accomplish this task.

For definitive purposes, a successful landing will be termed as any landing which satisfies certain impact constraints; namely, a near-zero velocity and a near-vertical orientation. From the results of an earlier study, a propulsive descent guidance law was developed and successful landings were realized when the mode of flight was gravity-turn and the engine thrust was modulated by the guidance law. The attitude control system satisfied the gravity-turn requirements by maintaining alignment between the thrust vector and the lander's negative velocity vector.

The guidance law developed may be expressed in the form

$$A = g_m + \frac{V^2}{2R} \tag{1}$$

where g_m is the Martian acceleration of gravity, R is the slant range, V is the surface-referenced velocity, and A is the instantaneous acceleration along the roll-axis required to soft-land. The descent system is mechanized such that the control loop compares the values of Eq. (1) with an on-board accelerometer and uses the error to adjust the throttleable engines.

Eq. (1) requires measurements of V and R throughout the descent. Range and velocity data can be obtained by implementing an on-board radar system similar to *Surveyor's* RADVS (radar altimeter doppler velocity sensor). The computation required in Eq. (1) will be performed by a computer which will be integrated in the descent system as shown in Fig. 2.

UNCLASSIFIED CONFIDENTIAL

UNCLASSIFIED
CONFIDENTIAL

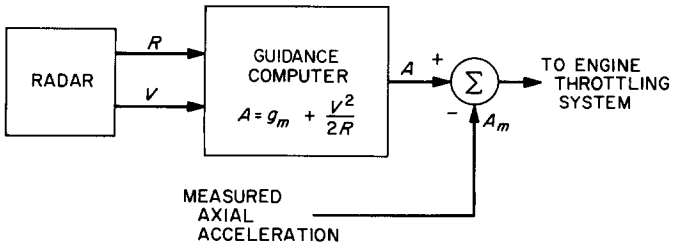

Fig. 2. Simplified terminal guidance system block diagram

In executing the terminal descent, stabilization and radar acquisition modes are required immediately after ignition. The former mode is necessary for alignment of the thrust vector and the latter necessary to obtain reliable velocity and slant range information. Several seconds of execution time are required by these modes.

A 2 degrees-of-freedom computer simulation, which integrated the equations of motion in the vertical descent plane, was developed to evaluate the feasibility of using the guidance law in Eq. (1) to control the descent. The equations of motion are obtained from the descent geometry shown in Fig. 3. It was assumed in the evaluation that all systems were ideal and that the modes required in this mechanization were not perturbed by imperfect executions.

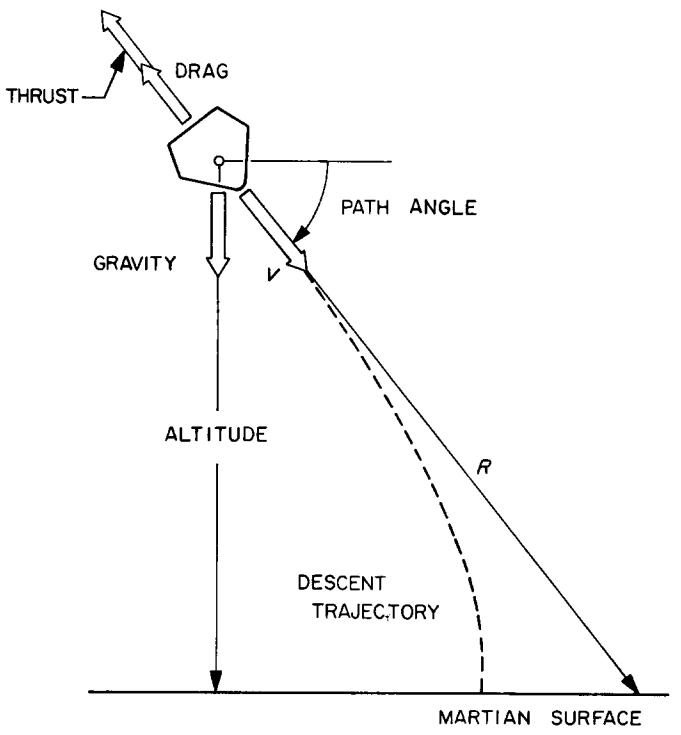

Fig. 3. Terminal descent geometry

The ignition conditions given in Table 1 were selected as the study cases. Results of these simulated descents showed that a "floating effect" occurred for the most dense atmosphere, VM-10. This was attributed to the high altitude, low velocity conditions at ignition. Long descent times resulted and the fuel consumption was dictated by VM-10, rather than VM-7, which requires the retro system to remove at least twice the velocity required by VM-10. For VM-7 and -8, no particular problem areas were observed in the flights. A conclusion based on these results is that a mode should be introduced in the guidance system that would reduce the fuel consumption in the more dense atmospheres and thus allow propulsion system sizing on the basis of the highest ignition velocity.

In the ensuing discussion, we will describe in detail how the guidance computer can be modified to incorporate a mode which will alleviate the excessive fuel requirements of the dense atmospheres.

6. Proposed Guidance System Mechanization

As stated earlier, the ignition altitude, as determined from the slant range ignition criterion, increases as the atmospheric density increases. Hence, to reduce the altitude to where the "floating effect" is essentially alleviated, it is desirable to delay control by Eq. (1) from ignition to some later time during the descent. During this period, the lander would descend at some minimum thrust, sufficient to maintain altitude control capability, to accomplish the altitude reduction. The velocity would also be reduced by the relatively small thrust force and the atmospheric drag acting on the lander. Furthermore, a minimal amount of fuel would be required to produce the necessary thrust.

It now remains to establish a criterion for instituting such a mode and to determine the duration of the mode. We will denote this mode as a minimum deceleration or "drop" mode. The duration is bounded by VM-7 and -10, minimum and maximum durations, respectively. A problem thus arises in defining the duration for the atmospheres between the bounds.

A typical set of vehicle acceleration boundaries computed from Eq. (1) and plotted as a function of slant range is shown in Fig. 4. If a continuous acceleration contour can be defined as an inverse function of slant range, a drop mode can be defined whose duration is proportional to the atmospheric density for any atmosphere between the VM-7 and -10 bounds. Such a contour is given in Fig. 4 as A_{con}. It may be described

CONFIDENTIAL
UNCLASSIFIED

UNCLASSIFIED
CONFIDENTIAL

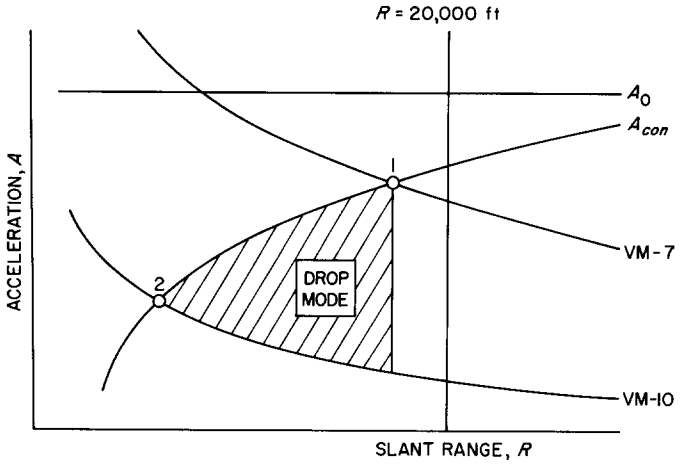

Fig. 4. Typical acceleration boundaries illustrating drop mode duration

mathematically as

$$A_{con} = A_0 - \frac{\alpha}{2R} \tag{2}$$

where A_0 is an asymptote of A_{con} whose value is determined from the maximum acceleration capability of the engines, R is the slant range, and

$$\alpha = 2Kg_m \tag{3}$$

K is a constant that shapes the contour such that the acceleration capability of the engines is not exceeded. From Fig. 4, it is seen that the drop mode is bounded by the ignition slant range, A_{con}, and the minimum acceleration characteristic. The region between $R = 20{,}000$ ft and the beginning of the drop mode is the duration of the stabilization and acquisition mode.

Since slant range data will be available, A_{con} can be computed. When A_{con} intersects the acceleration curve, Points 1 and 2 in the figure, the control is switched to Eq. (1). To establish this guidance policy, the following criterion may be stated:

When

$$A = A_{con} \text{ or } A_0 = \frac{V^2 + \alpha}{2R} + g_m \tag{4}$$

begin descent controlled by Eq. (1).

A block diagram of a digital computer containing this modification is shown in Fig. 5. The constants g_m, α, A_0, A_1, and A_2 are placed in data storage in the computer. A_1 is the acceleration required at ignition for stabilization and acquisition and A_2 is the minimum acceleration during the drop mode.

The computer operation may be briefly described as follows. The ignition signal activates a start mechanism in the computer and A is set equal to A_1. A_1 is sent to the output block where it is diverted to the thrust control loop and to the *if doppler reliable* block which denotes the end of stabilization and acquisition. When the doppler reliable signal occurs, computation of Eq. (4) begins. The computed value of A is then compared with A_0 and if $A < A_0$, the drop mode begins and A is set equal to A_2. The lander continues in the drop state until $A > A_0$, at which time α and A_0 are set to zero. The computed descent state is maintained until touchdown.

7. Simulated Flight Results

Terminal descent flights using the drop mode modification were simulated to determine the improvement over the previous technique. Of particular interest were the altitude-velocity profile and the fuel consumption-descent time characteristics. The flights were simulated using the ignition conditions of Table 1. Computer data storage constants were the following:

$$g_m = 12.33 \text{ ft/sec}^2$$

$$\alpha = 2.47 \times 10^5 \text{ ft}^2/\text{sec}^2$$

$$A_0 = 4\, g_m$$

$$A_1 = 1.5\, g_m$$

$$A_2 = 0.9\, g_m$$

Plots of altitude versus velocity are shown in Figs. 6 and 7. Descent time τ, and fuel consumption F, are presented as factors of the values of τ and F for VM-7. In each figure, the three distinct modes, where three are necessary, are very clearly illustrated. The fuel consumption data showed that in all cases the maximum fuel requirements were dictated by the VM-7 ignition conditions.

Based on these preliminary results, this guidance system appears to be a feasible mechanization which eliminates to a great extent the dependence of the descent system design on the relatively unknown Martian atmosphere. Further effort, such as more detailed studies which consider system perturbations, parametric optimization, and wind effects, would be required prior to committing a project to this mechanization.

UNCLASSIFIED
CONFIDENTIAL

UNCLASSIFIED
CONFIDENTIAL

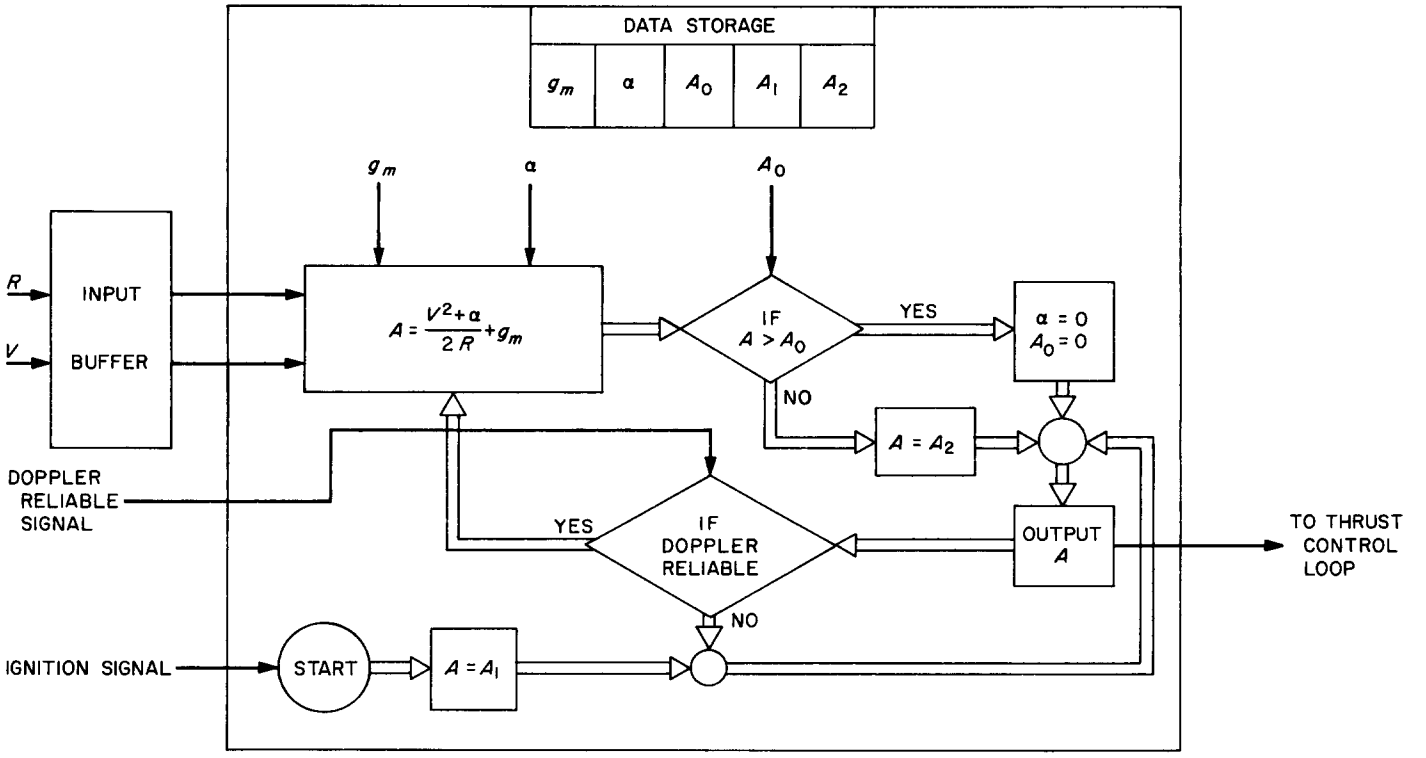

Fig. 5. Guidance computer mechanization

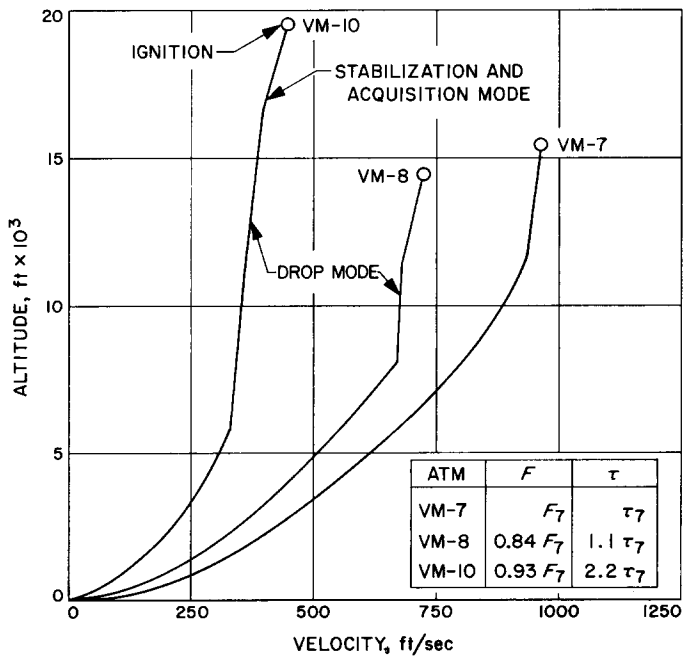

Fig. 6. Powered descent trajectories for an entry angle of −14 deg

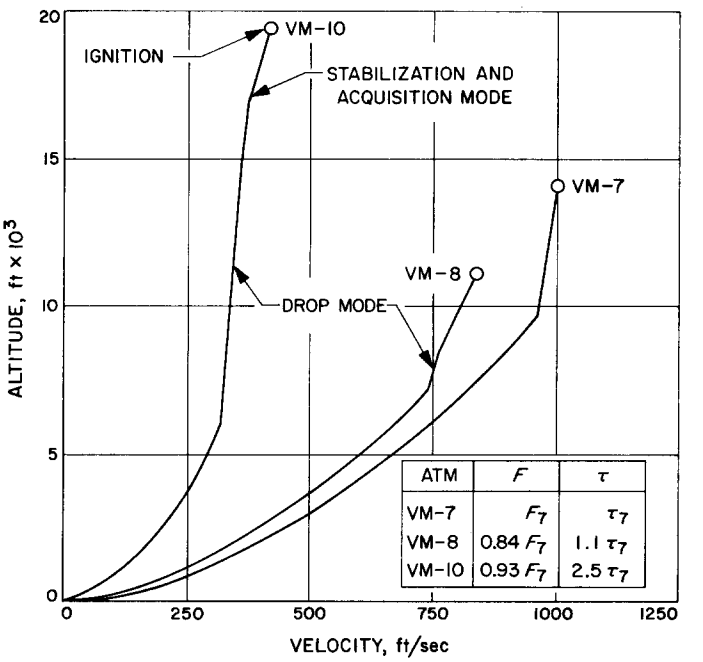

Fig. 7. Powered descent trajectories for an entry angle of −20 deg

CONFIDENTIAL
UNCLASSIFIED

UNCLASSIFIED
CONFIDENTIAL

V. Future Projects

A. Introduction

The Future Projects Office of the Laboratory is responsible for the direction, sponsorship and, in cooperation with other elements of the Laboratory, the origination of advanced mission and future project studies in the areas of interest and applicability to the Laboratory.

The objective of this effort is to insure that the preliminary technical information and plans for the various potential missions, together with the associated information on spacecraft systems, instrumentation systems, launching vehicle systems, resources, and schedule be available as required. This preliminary mission study information will be used primarily for defining specific flight mission programs, and as generalized guidance for the Laboratory research and advance development programs.

Each study conducted by the Future Projects Office has been, and will continue to be, documented in a formal final report. This section of the Space Programs Summary is allocated to provide an abstract or summary of the results of each study including, where appropriate, reference to final report for additional details.

B. A Comet Mission

This report describes several possible scientific objectives with their supporting experiments, and also provides some scientific information for a preliminary study of a comet mission to be undertaken during the period 1970–1976.

1. Mission Constraints

The launch vehicle assumed for this mission has at least the capabilities of an *Atlas/Centaur*. Because of the high injection energy requirements for most comet missions, and the relatively modest capability of the *Atlas/Centaur* launch vehicle, target selection is limited, as is also spacecraft weight and the resulting scientific payload. Even so, preliminary trajectory analyses indicate that there will be several very favorable comet apparitions for the period 1970–1976 that are most amenable to study from a lightweight *Mariner*-type spacecraft. These opportunities are expected to allow the consideration of 110 to 150 lb of scientific payload for a particular mission. This is certainly adequate, and a select list of scientific experiments on board an intercept probe of this

UNCLASSIFIED
CONFIDENTIAL

UNCLASSIFIED
CONFIDENTIAL

type can be expected to provide data toward a major advance in our understanding of comets.

In order to derive the maximum scientific value from a comet intercept probe, it is necessary to define several mission constraints that affect not only the choice of experiments and their unique requirements and techniques for implementation, but also the feasibility of the mission itself. These comet-mission constraints as presently conceived are as follows.

a. Intercept miss distance. A spacecraft–comet encounter miss distance of less than 2500 km is desirable. Through DSIF tracking and programmed trajectory corrections, the spacecraft location in space will be both known and, within limits, changeable; however, the comet's trajectory will not be as well known and so the precise point and time of spacecraft–comet encounter will be largely dependent upon knowledge of the comet's orbital elements. This suggests that a very extensive optical observation program of the comet will be necessary throughout the apparition – that is, for several weeks prior to spacecraft launch and during the flight portion of the mission. This further suggests that the selection of any particular comet for the mission should be limited to short periods whose orbital elements are already reasonably well known and which can be predicted to be bright enough to permit early recovery.

Previous studies of the trajectories, orbital determination techniques, and spacecraft guidance problems for a number of select comet missions have indicated that a 2500-km spacecraft–comet encounter miss distance is feasible. This is without the complication of an on-board comet-seeker for in-flight and terminal guidance. The general comet selection and guidance procedures for achieving this accuracy in flyby distance are envisioned as follows:

(1) Use the data from earlier apparitions of a number of selected short-period comets to determine their orbit, predict intercept point, etc., and select one as a likely target.

(2) Begin optical tracking of the comet from several facilities at its first appearance to determine a more precise orbit and intercept point. It is expected that this phase would begin several months before launch.

(3) Launch the spacecraft on the basis of (2) above.

(4) Track the spacecraft and the comet.

(5) Use midcourse and terminal corrections to achieve final rendezvous.

b. Intercept close to perihelion. Except for the rare annual comets such as Schwassmann-Wachmann 1, comets usually become visible as they approach the Sun and become influenced by solar radiation. Their most active period is near perihelion; therefore, it is desirable to have the spacecraft–comet intercept occur at, or near, perihelion passage. This is also an important consideration for the constraint to be discussed next.

c. Visible from Earth during intercept. It is very desirable that the comet be visible from Earth during the intercept phase to allow the correlation of data between the spacecraft scientific instruments and Earth observatory, and perhaps, orbiter observation. This places a requirement on both the brightness of the comet and its trajectory. Thus, any comet chosen for this mission should be a visual comet, or at the least, one that is capable of achieving a brightness magnitude of at least 10 during the intercept phase of the mission. This is especially desirable for carrying out any Earth-based spectroscopic observations. This is a difficult constraint; few periodic comets have been observed to "boilup" to a visual magnitude of, say 6.

d. Closing velocity. Closing velocities indicate how long the spacecraft will be in a particular comet and also affect the design of the scientific instruments, their data rate, and scan platform. In all cases, the comet overtakes the spacecraft. A low closing velocity is desirable, with the comet flying slowly by the spacecraft; however, a differential velocity of up to 50,000 ft/sec^{-1} would be acceptable.

e. Trajectory constraints for approach, fly-through, and recession of comet. It is desirable to fly through the coma and as close to the nucleus as possible in order to observe the central core of the comet. The desired trajectory is expected to pass through the coma, and as discussed earlier, to within 2500 km of the nucleus. Further, the trajectory should offer an opportunity to perform scientific experiments on the comet's coma and tail during the approach and recession portion of the flight. It should be noted that for most trajectories, the cometary tail cannot be intercepted on leaving the coma without a significant change in the course of the spacecraft.

f. Spacecraft hazard. The physical state and distribution of matter within a comet are largely unknown; thus, the actual coma penetration phase of this mission could involve a hazard to the spacecraft. For this reason, it may

UNCLASSIFIED
CONFIDENTIAL

UNCLASSIFIED
CONFIDENTIAL

be desirable to have certain critical spacecraft components shielded and also to have a real time or at least a high data rate transmission capability for monitoring the spacecraft engineering and scientific data. In this way, it may be possible to have information on a hazardous situation before loss of contact with the spacecraft. Fortunately, the intercept phase of most of the comet missions that are practical seems to occur when the communication distance is very small – say a few tenths of an astronomical unit. This could have a big advantage in sizing a communication link for a high data rate transmission.

g. Target selection. The selection of a specific comet for an intercept mission will not be attempted in this document. This can be accomplished only after a detailed analysis has traded off the above constraints for particular comets with technical data involving constraints on the launch vehicle, launch window, flight time, approach velocity, communication distance, guidance and control, and finally, the mission scientific objectives and their resulting scientific instruments.

2. Nature of Comets

The majority of comets remain telescopic objects only, but every 2 or 3 yr one appears sufficiently bright to be visible to the unaided eye (from some part of the Earth) while three or four times a century comets appear visible near the Sun, even in broad daylight. The latest of these was Ikeya-Seki in 1965, and there were previous daylight comets during this century, in 1910 and 1927. Despite the frequency of occurrence of comets, many problems connected with them may be unsolvable by ground-based observations, and this mission is concerned with the need for application to comets of the most modern astronomical tool of all, the space probe.

When first observed far from the Sun, a comet appears as a fuzzy area of light scarcely distinguishable from the background of the sky. As it approaches the Sun, it may appear to change in size in curious ways, and the brightest usually develops extensive tails stretching visibly more than 10^8 km from the comet itself. There is no doubt that material is lost from any comet at each return to the Sun, while dynamical effects can eject comets completely from the solar system. Such considerations suggest that comets may not be original members of the system but have been acquired from time to time since that epoch.

The observational information yet available has been of such a nature as to permit different theories of the structure of comets, and much speculation on their possible origin has also taken place. Many unsettled questions have developed that may only be capable of resolution by instrumentation passing within and near an actual comet. It is possible that comets form from interstellar dust, and if this is so they may provide accessible samples of this. In any event, knowledge of the chemical composition of cometary material would be highly desirable, as it may represent a closer estimate of the composition of galactic material than anything else in the solar system, and lead to important evidence on the origin of the elements.

The principal question as to the structure is whether comets are to be regarded in essence as small compact accumulations of ices and dust of kilometric dimensions, or as huge diffuse swarms of tiny particles measuring hundreds of thousands of kilometers in over-all dimensions. On either basis, interaction with the Earth, Moon, and other planets will have occurred, and this raises important questions as to the possible effect on the surfaces and atmospheres of such bodies.

Such properties of comets are known, and their orbital motions are in direct contrast with the corresponding properties of the planets, and this antithesis renders them almost equally important objects in the solar system from a cosmogonical standpoint. But it has to be admitted that comets remain very poorly understood, with much diversity of opinion, and as a result the selection of suitable and acceptable scientific objectives and experiments for a comet-intercept is not altogether an easy task. It is essential that crucial worthwhile experiments be devised, and for this reason alone it is desirable that the project be reviewed by a large section of the scientific community comprising many disciplines.

It is the thesis of this report that a *space probe to a comet* may be potentially the most important mission for purposes of cosmogonical research that will be within the capabilities of the decade 1971–1980.

3. Scientific Objectives and Experiments

The Space Science Board of the National Academy of Sciences has developed a rationale for exploration of the solar system. It states that the exploration of the solar system is concerned with three central scientific problems of our time, defined as: (1) the origin and evolution of the Earth, Sun, and planets (moons, asteroids, and comets implied); (2) the origin and evolution of life; and (3) the dynamical processes that shape man's terrestrial environment. In terms of these major problems, it has

UNCLASSIFIED
CONFIDENTIAL

UNCLASSIFIED
CONFIDENTIAL

further suggested a number of specific questions to guide cometary research.

Obviously, the mission under consideration in this document cannot logically be addressed to the task of answering all of the questions specified by the Space Science Board, so some ordering is required. It would seem that the important questions can be divided into two groups. The first group is concerned with questions regarding the physical nature and composition of the comet itself. For example, are cometary nuclei made up of single bodies of icy material, and if so, what compounds do the ices comprise? What is the chemical nature of the material? Is the so-called sand bank model appropriate, and if so, what is the nature and distribution of particles? The second group is concerned with questions regarding the interaction of the cometary matter with solar corpuscular and electromagnetic radiation, and with interplanetary magnetic fields. For example, how are tail gases ionized? How are they accelerated away from the Sun; if by solar wind, what is the coupling mechanism? What is the effect of cosmic ray bombardment?

From the foregoing, it seems appropriate that the scientific objectives for this preliminary mission study should be to investigate the comet at proximity with experiments designed to determine its physical state, structure, composition, and how it reacts to its environment. A select scientific payload to accomplish these broad objectives could be comprised of the following experiments: photo-imaging, mass spectrometer, dust detector, magnetic fields, plasma spectrometer, infrared interferometer, cometary mass, and space physics. The scientific objectives and some of the instrument characteristics for these particular experiments are given in Table 1.

Table 1. Scientific experiments

Experiment	Weight, lb	Power, w	Objective
1. Photo imaging	50	32 (maximum)	To examine the nucleus, if present, and determine its shape, size, albedo, and light-scattering properties, and also to examine the over-all structure of the comet and observe any temperal and spatial changes
2. Mass spectrometer	12	15 (maximum)	To investigate the chemical nature of the gaseous material making up the coma, and to determine the distribution of such species and ionized constituents as can be identified
3. Solid particles	10	2	To investigate the distribution, mass and velocity of small solid particles throughout the coma and in space
4. Magnetic fields (a 3-axis helium magnetometer plus a single-axis search coil magnetometer)	8	7	To examine magnetic fields in space and in the comet, and to investigate interaction between the comet and the ambient solar environment
5. Plasma spectrometer	20	10	To examine plasma streams in the comet and in space and to obtain data on the interaction that must occur between the solar plasma and the cometary atmosphere
6. Infrared interferometer	26	12	To examine at close range the gaseous envelope around the nucleus to decide on the origin of the radicals C_2, CN, etc.
7. Cometary mass	NA	NA	To determine mass of cometary nucleus as may be indicated by tracking data
8. Space physics (a) Particle flux/ion chamber	2.5	>1	To measure the total ionizing radiation in space and around and through the comet, and to provide semiquantitative information about the energy and particle types composing the radiation
(b) Medium energy-range particle detector	2.5	>1	To extend the range of the plasma experiment for detecting electrons and protons in space and throughout the comet
(c) Bistatic radar	12	5	To investigate electron density in space and in the comet and obtain data on radar cross section and other properties of the comet

UNCLASSIFIED
CONFIDENTIAL